Check for updates

ADVANCED FUNCTIONAL MATERIALS
www.afm-journal.de

PNIPAM/PEDOT:PSS Hydrogels for Multifunctional Organic Electrochemical Transistors

Naroa Lopez-Larrea, Shofarul Wustoni, Mario Iván Peñas, Johana Uribe, Antonio Dominguez-Alfaro, Antonela Gallastegui, Sahika Inal, and David Mecerreyes**

The development of multifunctional organic materials represents a vibrant area of research, with applications spanning from biosensing to drug delivery. This study shows the development of a multifunctional bioelectronic device suitable for prolonged temperature monitoring and drug delivery applications. The device relies on a conducting and thermo-responsive hydrogel made of poly(3,4-ethylenedioxythiophene) doped with poly(styrene sulfonate) (PEDOT:PSS) and poly(N-isopropylacrylamide) (PNIPAM). This multifunctional hydrogel is 4D printable by Digital Light Processing (DLP) method and exhibits optimal biocompatibility. The hydrogel features a low critical solution temperature (LCST) ≈35 °C, above which its resistance changes dramatically due to the shrinkage it undergoes with temperature. The integration of PNIPAM/PEDOT hydrogel into an organic electrochemical transistor (OECT) as the gate electrode allows to generate a miniaturized bioelectronic device with a reversible response to temperature variations between 25 to 45 °C, along with high sensitivity of 0.05 °C^{-1}. Furthermore, the PNIPAM/PEDOT hydrogel demonstrates its utility in drug delivery, achieving an Insulin-FITC release rate of 82 ± 4% at 37 °C, mimicking human body conditions. The hydrogel's functionality to store and release the insulin does not compromise its thermo-responsivity and the overall performance of the OECT. This multifunctional OECT opens new avenues for the development of customizable and personalized sensing and drug-delivery systems.

1. Introduction

Organic electrochemical transistors (OECTs) have become prominent as versatile bioelectronic devices in wearable electronics, neuromorphic computing, chemical and biological sensing.[1] These applications benefit from OECTs' features, such as high transconductance, chemical stability and biocompatibility and soft mechanical contact with the biological system.[2] The OECTs-based transducer offers high amplification capability which can detect small input signals into large readable output responses with a high signal-to-noise ratio.[3,4] OECT comprises three primary components: the gate electrode, the semiconducting polymer channel and the electrolyte, each pivotal to the electrical performances and stability of the transistor. While significant efforts have been made in developing OECTs for various chemical and biosensors through functionalization of the gate and/or channel with different receptor units,[5–7] the exploration of thermo-responsive OECTs remains relatively uncharted. The development of thermo-responsive OECTs could be further integrated as miniaturized and localized temperature sensors in various bioelectronics, such as implantable microelectrode arrays, wearable multiplex sensors, and temperature monitoring at the cell level.

Temperature is a critical parameter in biological processes with variations often indicative of physiological activities at the cellular level and pathological conditions such as tumor tissue

N. Lopez-Larrea, M. I. Peñas, A. Dominguez-Alfaro, A. Gallastegui, D. Mecerreyes
POLYMAT and Department of Polymers and Advanced Materials: Physics, Chemistry and Technology
Faculty of Chemistry
University of the Basque Country UPV/EHU
P Manuel de Lardizabal 3, Donostia-San Sebastian 20018, Spain
E-mail: david.mecerreyes@ehu.es

The ORCID identification number(s) for the author(s) of this article can be found under https://doi.org/10.1002/adfm.202403708

© 2024 The Authors. Advanced Functional Materials published by Wiley-VCH GmbH. This is an open access article under the terms of the Creative Commons Attribution License, which permits use, distribution and reproduction in any medium, provided the original work is properly cited.

DOI: 10.1002/adfm.202403708

S. Wustoni, J. Uribe, S. Inal
Organic Bioelectronics Laboratory, Biological and Environmental Science and Engineering Division
King Abdullah University of Science and Technology (KAUST)
Thuwal 23955-6900, Saudi Arabia
E-mail: sahika.inal@kaust.edu.sa

M. I. Peñas
Institute of Polymer Science and Technology ICTP-CSIC
Juan de la Cierva 3, Madrid 28006, Spain

D. Mecerreyes
IKERBASQUE
Basque Foundation for Science
Bilbao Spain

16163028, 2024, 40, Downloaded from https://onlinelibrary.wiley.com/doi/10.1002/adfm.202403708 by Universidad Del Pais Vasco, Wiley Online Library on [08/10/2024]. See the Terms and Conditions (https://onlinelibrary.wiley.com/terms-and-conditions) on Wiley Online Library for rules of use; OA articles are governed by the applicable Creative Commons License

exhibiting higher temperatures than healthy tissue.[8] Conventional temperature sensors, such as mercury and infrared thermometers, fall short in the nuanced needs of integrated, miniaturized and localized temperature measurements for disease diagnosis and treatment. Simultaneously, advancements in drug delivery technologies have been proven to improve treatment outcomes in many ways, including enhancing therapeutic efficacy, increasing patient compliance and enabling entirely new medical treatments.[9] To date, there is a great interest in developing bioelectronic devices that combine functionalities of temperature sensitivity with drug delivery capabilities paving the way for customizable medicine.

Conductive hydrogels, particularly those based on poly(3,4-ethylenedioxythiophene): poly(styrene sulfonate) (PEDOT:PSS), stand out in bioelectronics for their superior electronic conduction, ion transport capability, biocompatibility and stability in complex biological media.[10–14] Nonetheless, creating PEDOT-based hydrogels remains a difficult challenge, demanding a delicate balance between maintaining the PEDOT's inherent electrical conductivity while incorporating the desirable features of hydrogels such as tuneable mechanical properties.[15–17] On the other hand, the possibility of processing them by 3D printing techniques is still under investigation including direct ink writing (DIW),[18–22] light-based 3D printing (stereolithography and digital light processing, SLA and DLP)[23–30] and extrusion-based printing.[31–34] The fabrication of 3D PEDOT-based hydrogels at high resolutions opens new opportunities for customizable and intricate materials. However, the quest for stimuli-responsive and multifunctional PEDOT-based hydrogels continues, driven by the need for complex, patient-specific bioelectronic devices.[35]

Incorporating multifunctionality into PEDOT-based hydrogels could be achieved by combining them with stimuli-responsive hydrogels (SRHs), smart hydrogels capable of responding to external environmental stimuli such as temperature, pH, near-infrared light, electrical fields, magnetic fields, humidity or pressure and converting these stimuli into desired functions.[36] The advantage of SRHs is that they can be processed by 4D printing combining the previously mentioned 3D printing techniques with the induced shape morphing effect in response to external stimuli as the 4th dimension, uncovering new advancements in the additive manufacturing (AM) field.[37] Among these SRHs, temperature-responsive hydrogels have gained immense attention over the years in bioengineering, particularly for drug delivery and photothermal therapy applications, due to their rapid and precisely controllable responses.[38] The most common material for the synthesis of temperature-responsive hydrogels is poly(N-isopropylacrylamide) (PNIPAM), a polymer that exhibits temperature sensitivity with a lower critical solution temperature (LCST) close to human body temperature, enabling swelling/deswelling and absorption/desorption in response to temperature changes.[39] Therefore, recent research has begun to explore further the conductive hydrogels that merge the electrical conductivity of conducting polymers with the thermo-responsive characteristics of PNIPAM, acquiring versatile platforms with additional functionalities.[40–47] This versatility was demonstrated in recent studies, such as Garcia-Hernando et al.'s work, which incorporated PNIPAM with PEDOT:PSS to create a smart copolymer for label-free, non-invasive detection of cell capture and release on gold electrodes via electrochemical impedance spectroscopy.[48] In another example, Liu et al. developed a series of polyaniline/poly(styrene-co-N-isopropylacrylamide) (PANI/P(St-NIPAM)) composites through seeded PANI polymerization within sulfonated P(St-NIPAM) particles, endowing these materials with temperature-responsive and electrical conductivity switch ability characteristic.[49] Despite these advancements, the examples above predominantly involve 2D form factor, highlighting ongoing challenges and drawbacks in creating 4D printable multifunctional conductive hydrogels. Issues such as stability or printability must also be addressed to facilitate broader adoption. Furthermore, finding an optimal balance between electrical conductivity and thermo-responsiveness remains challenging and requires meticulous optimization in material design. Moreover, integrating these smart hydrogels with OECTs remains a limited area of exploration.

This article presents the synthesis of 4D printable multifunctional PNIPAM/PEDOT conductive hydrogels for creating thermo-responsive OECTs. The photopolymerization process of the NIPAM monomer with varying concentrations of PEDOT:PSS is detailed, as well as the processability of these hydrogels by DLP method. In addition, comprehensive characterizations to assess the impact of PEDOT:PSS concentration on the physical, chemical, and electrochemical properties of the hydrogels are conducted. As an application, the best-performing PNIPAM/PEDOT hydrogel was integrated into an OECT as the gate electrode, examining its performance, thermal responsivity, and stability. Finally, the hydrogel's drug release capabilities was assessed using Insulin-FITC at different temperatures, alongside its influence on the thermo-responsivity of the OECT. The integration of thermo-responsive OECT sensors with insulin delivery system represents a unique approach to leverage the interplay between temperature fluctuation, glucose level, and insulin delivery processes.[50–54] This multi-task OECT represents a significant step forward in the development of multifunctional bioelectronic devices for medical advances.

2. Results and Discussion

2.1. Design of Photopolymerizable Inks for 4D Printing of PNIPAM/PEDOT:PSS Hydrogels

A schematic representation of the overall fabrication process for multifunctional 4D printable PNIPAM/PEDOT hydrogels is depicted in **Figure 1**. Initially, the N-isopropylacrylamide (NIPAM) monomer was dissolved in varying concentrations of PEDOT:PSS aqueous solutions (0, 0.5 and 1.3 wt.%).[55,56] Then, poly(ethylene glycol diacrylate) as a cross-linker and a commercial photoinitiator were added to the NIPAM/PEDOT mixtures. Afterward, the pre-polymeric inks underwent sonication at 30 °C for 15 min to ensure a homogeneous solution, as the NIPAM solubility in water is low at room temperature (212 ± 8.56 mg mL^{-1}). Finally, the hydrogels were formed by the photopolymerization of the inks employing UV light, resulting in a crosslinked PNIPAM network encapsulating the PEDOT:PSS chains (Figure 1a).

The quest for multifunctional materials capable of being processed by Digital Light Printing (DLP) into complex structures is vigorous within the bioelectronics field.[24,57] DLP is favored 3D printing method for its high-resolution capabilities, cost-effectiveness and user-friendly operation.[58,59] To evaluate the

© 2024 The Authors. Advanced Functional Materials published by Wiley-VCH GmbH

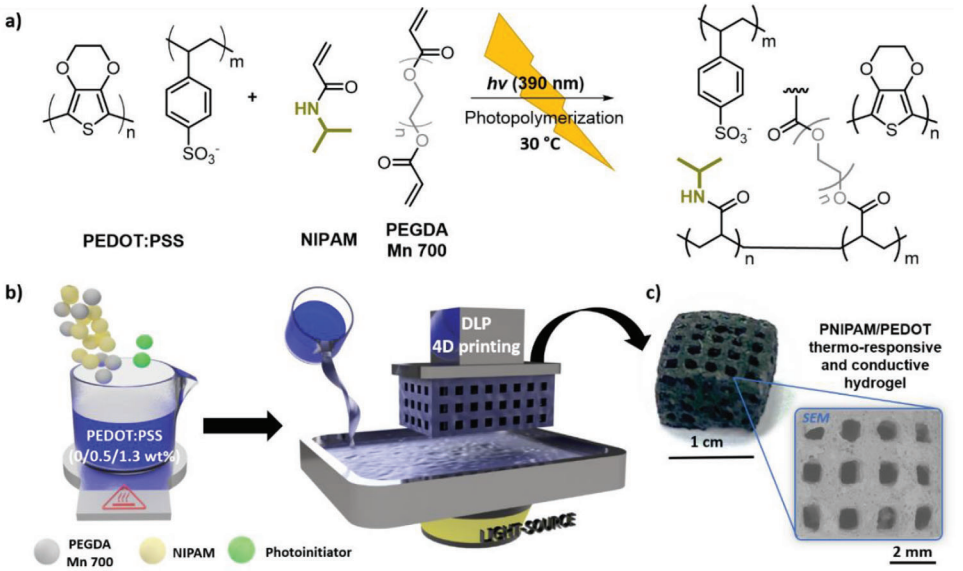

Figure 1. a) Synthesis of PNIPAM/PEDOT hydrogels by photopolymerization reaction, b) Fabrication of photopolymerizable inks and shape-defined PNIPAM/PEDOT hydrogels by DLP 3D printing technique, and c) Macroscopic and SEM pictures of the printed thermo-responsive and conductive scaffold-shape hydrogel.

processability of the formulated inks, a systematic analysis of the photopolymerization reaction kinetics and ink viscosity was conducted to assess the impact of varying PEDOT:PSS concentrations on these parameters. The kinetics were monitored via Fourier Transform Infrared Spectroscopy (FTIR), tracking the decrease of the C = C out-of-plane bending vibration (vinylic peak) of the NIPAM monomer at 955 and 985 cm^{-1} under UV light irradiation, during the progression of photopolymerization reaction (Figure S1a, Supporting Information). The conversion was calculated using Equation 1 by measuring the area of these peaks over time. As observed in Figure S1b (Supporting Information), full conversion is achieved in less than one minute for all the formulations, despite the PEDOT:PSS absorption in the UV–vis spectrum,[60] which could potentially affect the kinetics, proving the effectiveness of the chosen photoinitiator (see experimental section).[26] Therefore, the rapid photocuring speed renders these inks highly suitable for the DLP technique. However, this printing method not only needs fast photopolymerization kinetics, but also needs to maintain a viscosity of the inks below 20 Pa s at a shear rate of 10 to 100 s^{-1} to facilitate flow through the printer's vat.[61,62] Figure S2 (Supporting Information) shows the viscosity of different pre-polymeric solutions containing various amounts of PEDOT:PSS (0, 0.5 and 1.3 wt.%). It can be appreciated that as the concentration of PEDOT:PSS in the ink increases, the viscosity also increases, but all of them meet the requirement to be processed by a DLP 3D printer.

Therefore, DLP was used to pattern PNIPAM/PEDOT hydrogels with pre-designed architectures during the photopolymerization process, leading to 3D shape-defined network structures (Figure S3a,b, Supporting Information). PNIPAM/PEDOT (1.3 wt.%) ink was deposited in the commercially available DLP 3D printer vat, and through a layer-by-layer light irradiation in the Z axis, the pre-polymeric solution was photopolymerized on the platform, successfully obtaining the conductive and thermo-responsive hydrogel (Figure 1b). A layer height of 0.1 mm and exposure time of 30 s were applied as the optimal printing conditions. Figure 1c shows a macroscopic and SEM pictures of the shape-defined printed scaffold with a 500 µm hole size. In addition, a resolution test was carried out in order to determine the maximum x, y and z resolution of the 3D printed thermo-responsive hydrogel. For this purpose, a standard model with holes of 1000, 500, 250 and 100 µm was designed with Autodesk Inventor 2022 software (Figure S4a, Supporting Information) and, subsequently, the thermo-responsive material was printed (Figure S4b, Supporting Information). Besides, Figure S4c (Supporting Information) shows the magnifications of the holes in the 3D printed figure. It can be appreciated that the maximum x-y resolution is of 100 µm, a resolution needed for application in bioelectronics. On the contrary, the printing layer height, in this case 0.1 mm, determines the z-axis resolution. The high printing resolution shows the remarkable ability of these materials to be used in bioelectronic devices, where µm magnitudes are sought for microchips or OECTs.

2.2. Physicochemical Characterization, Biocompatibility Test and Thermal-Responsiveness of PNIPAM/PEDOT:PSS Hydrogels

The mechanical properties of hydrogels were analyzed through dynamic mechanical analysis (DMA) (Figure S5a–d, Supporting Information). It can be appreciated that bending storage modulus (G') and loss modulus (G'') do not intersect between them, indicating that the hydrogels exhibit a solid-like behavior across all measured frequencies and that they are fully crosslinked. Notably, the incorporation of PEDOT:PSS significantly enhances the mechanical properties, with the bending storage modulus (G') increasing from 2.7E+07 Pa to 1.1E+09 Pa (at 1 Hz frequency and 25 °C), resulting in a stiffer material as the

© 2024 The Authors. Advanced Functional Materials published by Wiley-VCH GmbH

16163028, 2024, 40, Downloaded from https://onlinelibrary.wiley.com/doi/10.1002/adfm.202403708 by Universidad Del Pais Vasco, Wiley Online Library on [08/10/2024]. See the Terms and Conditions (https://onlinelibrary.wiley.com/terms-and-conditions) on Wiley Online Library for rules of use; OA articles are governed by the applicable Creative Commons License

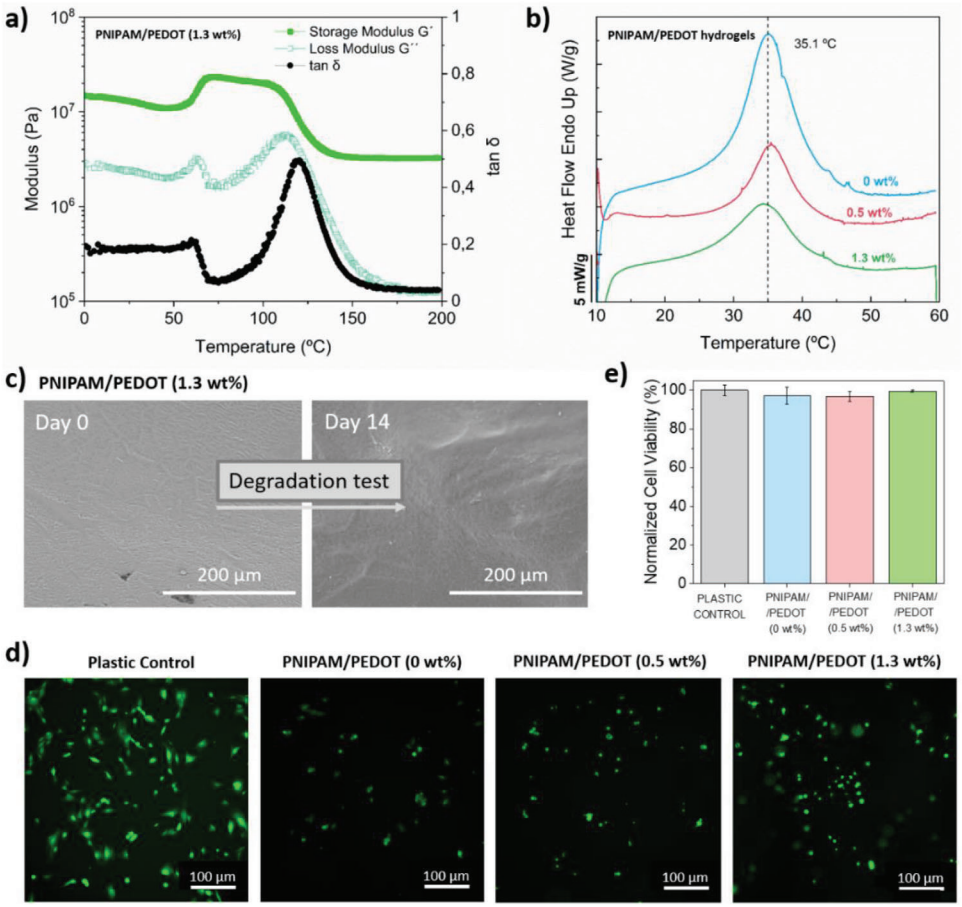

Figure 2. a) DMTA of PNIPAM/PEDOT (1.3 wt.%) hydrogel performed at 10 °C min^{-1}, b) Micro-DSC heating for PNIPAM/PEDOT (0, 0.5 and 1.3 wt.%) hydrogels performed at 0.2 °C min^{-1}, c) SEM images of PNIPAM/PEDOT (1.3 wt.%) hydrogel surface before and after degradation test, d) Fluorescent images of viable murine myoblast cells (C_2C_{12}) stained with Calcein-AM (green) on different substrates (polystyrene control and PNIPAM/PEDOT 0, 0.5 and 1.3 wt.% hydrogels) after 24 h of culture and e) Cell viability of C_2C_{12} after 24 h of culture on different samples (plastic control and PNIPAM/PEDOT 0, 0.5 and 1.3 wt.% hydrogels) normalized to the polystyrene positive control.

concentration of PEDOT:PSS within the polymer matrix rises. In addition, **Figure** 2a shows dynamic mechanical thermal analysis (DMTA) of PNIPAM/PEDOT (1.3 wt.%) hydrogel. The analysis reveals two main characteristics of PNIPAM hydrogels: i) an increase in both the compression storage modulus (G') and loss modulus (G'') ≈50 °C, corresponding to the low critical solution temperature (LCST) of the PNIPAM matrix, and ii) the maximum value for *tan δ* ≈125 °C, associated with the glass transition temperature (T_g) of PNIPAM matrix.[63] The absence of an intersection between G' and G'' at the T_g suggests effective crosslinking within the PNIPAM/PEDOT (1.3 wt.%) hydrogel, facilitated by the addition of PEGDA, thus enabling the hydrogel to absorb and retain water without being dissolved in the solution.

The shift in LCST to higher temperatures, as observed in the DMTA conducted at a rate of 10 °C min^{-1}, contrasts with literature values, prompting further investigation through micro-DSC at a rate of 0.2 °C min^{-1} to accurately determine the LCST.[64] Figure 2b shows the micro-DSC heating curves of all the different hydrogels, revealing endothermic peaks at 35.1, 35.4 and 34.7 °C for the PNIPAM/PEDOT (0, 0.5 and 1.3 wt.%) hydrogels, respectively. These thermal transitions are ascribed to the LCST of PNIPAM/PEDOT hydrogels, thus not being affected by PEDOT:PSS concentration as the conductive polymer merely occupies the 3D structure without altering the PNIPAM matrix. In order to confirm that the LCST signal comes only from the PNIPAM matrix, the commercial PEDOT:PSS was also analyzed, showing a lack of signal under identical conditions (Figure S6a, Supporting Information). This behavior has also been reported in literature, where PNIPAM solutions exhibited larger transitions (i.e., higher enthalpies) as the concentration of PNIPAM increased.[65] In addition, PNIPAM/PEDOT hydrogels start to undergo the reversible phase change from hydrophilic state to hydrophobic state from 20 to 50 °C, a broad phase change range if we compare with pristine PNIPAM of 21 450 g mol^{-1} molecular weight synthetized by free radical polymerization (see Figure S7a,b, Supporting Information), which demonstrates a more confined phase change range from 29 to 35 °C and the LCST at 31.7 °C (Figure S6a, Supporting Information). This effect of high LCST and broad phase range in PNIPAM/PEDOT hydrogels may be due to the copolymerization of PNIPAM with PEGDA cross-linker to form the polymer matrix.[66,67] When PEDOT:PSS is added to PNIPAM to form the hydrogels, the enthalpy associated to the LCST

© 2024 The Authors. Advanced Functional Materials published by Wiley-VCH GmbH

16163028, 2024, 40, Downloaded from https://onlinelibrary.wiley.com/doi/10.1002/adfm.202403708 by Universidad Del Pais Vasco, Wiley Online Library on [08/10/2024]. See the Terms and Conditions (https://onlinelibrary.wiley.com/terms-and-conditions) on Wiley Online Library for rules of use; OA articles are governed by the applicable Creative Commons License

transition (ΔH_{LCST}) is drastically decreased from ≈52 to ≈20 J g^{-1} (Figure S6b, Supporting Information), probably due to the presence of PEDOT:PSS, which can be preventing PNIPAM's LCST transition even at low concentrations. This behavior could be related to the addition of PEDOT:PSS into the PNIPAM matrix, which resulted in a decreasing response of thermo-responsivity, as evidenced by the reduction of the LCST's enthalpy observed by micro-DSC. This effect could be ascribed to the hydrophobic nature of PEDOT:PSS. Similar results were observed in aqueous solutions of PNIPAM copolymerized with acrylamide, where the enthalpy of the transition was reduced by ≈70% with the incorporation of acrylamide to PNIPAM.[68] The observed enthalpy associated to this transition of the pristine PNIPAM sample (48.6 J g^{-1}) is quite similar to that of PNIPAM/PEDOT (0%) sample (52.0 J g^{-1}). These results further support that the LCST signal is only due to PNIPAM. The fact that these hydrogels have the LCST at 35 °C makes them ideal candidates to be integrated in the body for drug delivery applications.

The durability of PNIPAM/PEDOT hydrogels was assessed in PBS at 37 °C to stimulate human body conditions.[69] Results shown in Figure S8a (Supporting Information) illustrate that the hydrogels exhibit remarkable stability, retaining over 90% of their initial weight after 2 weeks. In addition, Figures 2c and S8b (Supporting Information) highlight the morphological changes observed in the different hydrogels during the degradation test. Despite no significant weight loss, the hydrogels' morphology at the beginning of the test and 2 weeks later is different, being more wrinkled when exposed to the test conditions. This morphological change can be attributed to the phase change that hydrogels undergo near LCST temperature. Additionally, the thermal stability of PNIPAM/PEDOT hydrogels was also evaluated, revealing complete degradation at 450 °C (Figure S9, Supporting Information). These findings confirm the stability of these hydrogels for internal body applications.

In compliance with the ISO 10993–5, the biocompatibility of materials used in medical devices should be tested via, direct contact, extract, and/or indirect contact with the test sample.[70,71] Here, a general assessment of the biocompatibility of PNIPAM/PEDOT hydrogels is performed by testing the cytotoxicity of murine myoblast cells (C_2C_{12}), a popular cell line used in studies with scaffolds containing conductive polymers,[72–74] in direct contact with the hydrogels using a LIVE/DEAD assay. Figure 2d shows that all cells are viable (green signal) on the different hydrogels and on the control sample (cell culture polystyrene) after 24 h of cell culture. Interestingly, fluorescent images show that cell adhesion to the substrates increases as the PEDOT:PSS concentration increases in the hydrogels, which may be due to the increase in the storage modulus that takes place with the addition of PEDOT:PSS.[75] Besides, several works suggests that conductive polymers doped with anions can enhance cell adhesion and growth of various cells, supporting the improved adhesion of C_2C_{12} (myoblasts) cells as the percentage of PEDOT increases in the PNIPAM/PEDOT hydrogels.[76–79] As expected, the adhesion of the cells on the PNIPAM/PEDOT hydrogels is significantly lower than the adhesion on the polystyrene positive control. Myoblast confluence (%) for polystyrene positive control and PNIPAM/PEDOT (0, 0.5 and 1.3 wt.%) hydrogels was determined to be 50%, 15%, 33%, and 40%, respectively. This could be due to the phase change and morphological change that the hydrogels undergo at 35 °C, which can affect cell adhesion. In addition, it is well known that cells form larger and mature adhesions on stiff substrates compared to soft one caused by an increase in tension.[80,81] Although the cell adhesion on PNIPAM/PEDOT hydrogels is relatively low compared to the polystyrene positive control, normalized cell viability (i.e., relation of live and dead cells) is nearly 100% in all the samples (Figure 2e). The fact that cell viability in all the PNIPAM/PEDOT hydrogels is higher than 70%, makes the substrates non-cytotoxic, meeting the biocompatibility standards required for their integration into biomedical devices in compliance with ISO 10993–5.[71] In order to verify the non-cytotoxicity of the PNIPAM/PEDOT hydrogels, lactate dehydrogenase (LDH) assay was also performed to the materials using C_2C_{12} (myoblasts) cell line once again, and lysed cells as negative control. Figure S10 (Supporting Information) shows the cytotoxicity (%) values for PNIPAM/PEDOT (0, 0.5 and 1.3 wt.%) hydrogels after 24 h of cell incubation into the hydrogel's extracts media. As expected from the LIVE/DEAD test, the hydrogels are non-cytotoxic as they have a cytotoxicity (%) value smaller than 30%.

It is expected that PNIPAM/PEDOT hydrogels possess stimuli-responsive properties due to the presence of PNIPAM, which modulates their swelling behavior. **Figure 3a** displays a 3D printed lotus blossom with one part made of PNIPAM/PEDOT hydrogel and the other composed only of PEGDA. At 25 °C in a water solution, both blossom components appear hydrated. However, at 45 °C, above the LCST, the PNIPAM/PEDOT hydrogel contracts due to deswelling, making this material an example of 4D printing. This stimuli-responsivity of PNIPAM/PEDOT hydrogels was further explored by analyzing changes in swelling ratio, contact angle, tensile strength and surface morphology with temperature variations. Figure 3b depicts how the swelling ratio of different PNIPAM/PEDOT hydrogels changes with temperature from 25 to 45 °C. As the concentration of PEDOT:PSS increases in the system, the swelling ratio at 25 °C decreases from 525 ± 70% to 240 ± 8% for PNIPAM/PEDOT (0 and 1.3 wt.%) hydrogels, respectively, attributable to the hydrophobicity of PEDOT:PSS component. This reduction in the swelling of the hydrogels and the reduction in enthalpy observed for the LCST transition (as commented before in Figure 2b) has also been stated in literature for PNIPAM copolymers in solution with PEDOT:PSS, where the presence of PEDOT:PSS hindered the aggregation of the PNIPAM copolymer, which was responsible of the endothermic transition peak.[82] Moreover, as the water solution temperature where the hydrogels are immersed increases, the PNIPAM/PEDOT hydrogels begin to de-swell and completely dry at 40 °C. The possession of this significant phase change in the temperature range can be advantageous as it works not only at temperatures close to the LCST, but also across a broad temperature spectrum from 10 °C below and above the LCST.[83,84]

This shrinkage behavior that PNIPAM/PEDOT hydrogels exhibit is because of the reversible phase change that they possess, where they pass from a hydrophilic state to a hydrophobic state in the 25 – 45 °C range. This phase transition is evidenced by the contact angle measurement of PNIPAM/PEDOT (1.3 wt.%) hydrogel at 25 and 45 °C by placing a 10 µL droplet of distilled water on the hydrogel surface. The contact angle increases from

© 2024 The Authors. Advanced Functional Materials published by Wiley-VCH GmbH

16163028, 2024, 40, Downloaded from https://onlinelibrary.wiley.com/doi/10.1002/adfm.202403708 by Universidad Del Pais Vasco, Wiley Online Library on [08/10/2024]. See the Terms and Conditions (https://onlinelibrary.wiley.com/terms-and-conditions) on Wiley Online Library for rules of use; OA articles are governed by the applicable Creative Commons License

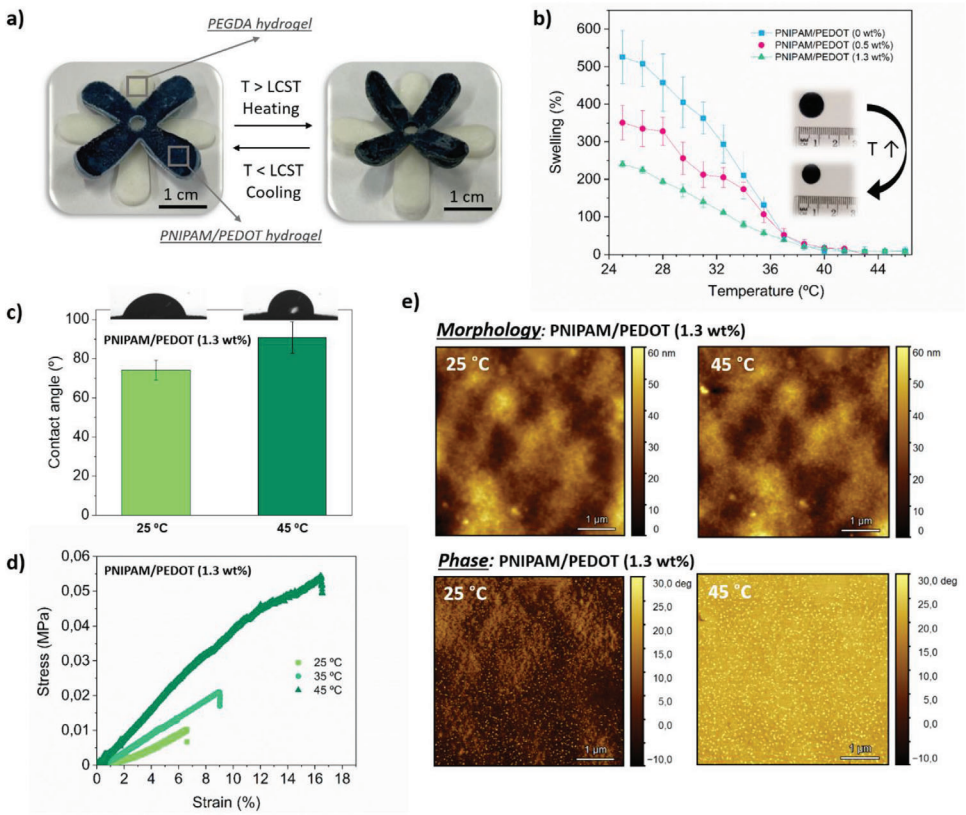

Figure 3. a) Stimuli-responsivity of PNIPAM/PEDOT (1.3 wt.%) hydrogel and PEGDA hydrogel with 3D printed lotus blossom's shape, below and above its LCST (35 °C), b) Swelling ratio of different PNIPAM/PEDOT (0, 0.5 and 1.3 wt.%) hydrogels versus temperature and a picture of the shrinkage of the materials with temperature increase, c) Contact angle of PNIPAM/PEDOT (1.3 wt.%) hydrogel at 25 and 45 °C with the corresponding droplets of distilled water, d) Stress–strain curves of type V probes' printed PNIPAM/PEDOT (1.3 wt.%) hydrogel at different temperatures (25, 35 and 45 °C) and e) AFM topographic height (morphology) and phase images of PNIPAM/PEDOT (1.3 wt.%) hydrogel at 25 and 45 °C.

74 ± 5 ° (at 25 °C) to 91 ± 8 ° (at 45 °C) (Figure 3c), indicating a transition from a hydrophilic state (° < 90) to a hydrophobic state (° > 90). Figure 3d shows the stress-strain curves of the PNIPAM/PEDOT (1.3 wt.%) hydrogel to varying temperatures with Type V probe shape obtained from the tensile test experiment. As the hydrogel shrinks with the increase in temperature, the Young's Modulus also increases from 0.19 ± 0.04 MPa to 0.46 ± 0.04 MPa for 25 and 45 °C, respectively (Figure S11, Supporting Information). Similarly, elongation at break increases from 6.6 ± 2% to 15.2 ± 1.8% with the temperature increase, obtaining more flexible materials as water is expelled from the polymer matrix. Finally, the surface topology of PNIPAM/PEDOT (1.3 wt.%) hydrogel was characterized by AFM at five different temperatures (25, 30, 35, 40 and 45 °C). Figures 3e and S12 (Supporting Information) shows the AFM morphology and phase of PNIPAM/PEDOT (1.3 wt.%) hydrogel surface at different temperatures. The AFM analysis shows minimal changes in surface morphology but a significant phase shift of nearly 30 degrees, linking to the change in mechanical properties and Young's modulus. These results revealed that the stimuli responsivity of PNIPAM/PEDOT hydrogels affects not only the shape change, but also the mechanical properties, swelling ratio and hydrophilicity, which can be advantageous in some applications such as drug delivery.

2.3. Electrochemical Characterization of PNIPAM/PEDOT:PSS Hydrogels

Theoretically, changes in the PNIPAM/PEDOT hydrogels' conductivity around their LCST are anticipated.[48,49] For this reason, the electrochemical properties of all hydrogels were studied across a temperature range of 25 to 45 °C. Electrochemical impedance spectroscopy (EIS) was used to characterize the electrochemical resistance of PNIPAM/PEDOT hydrogels, alongside control samples including gold electrode used as the substrate and a pristine PEDOT:PSS film coated as a 2D film on the gold substrate. These measurements were conducted in PBS to stimulate physiological conditions. The Bode plots and Nyquist plots of PNIPAM/PEDOT (1.3 wt.%) hydrogel are shown in **Figure** 4a,b, respectively (see Figures S13 and S14, Supporting Information for the other samples). The increase in solution temperature causes a decrease in the impedance magnitude and a shift of the phase spectrum toward higher frequencies with a decrease in its value. The Nyquist plots reveal a semicircle whose diameter narrows as temperature rises. On the contrary, neither the gold electrode substrate nor the pristine PEDOT:PSS in the absence of PNIPAM or PNIPAM/PEDOT (0 wt.%) hydrogel have any significant temperature induced-change in their impedance spectra (Figures S13 and S14, Supporting Information). These

© 2024 The Authors. Advanced Functional Materials published by Wiley-VCH GmbH

16163028, 2024, 40, Downloaded from https://onlinelibrary.wiley.com/doi/10.1002/adfm.202403708 by Universidad Del Pais Vasco, Wiley Online Library on [08/10/2024]. See the Terms and Conditions (https://onlinelibrary.wiley.com/terms-and-conditions) on Wiley Online Library for rules of use; OA articles are governed by the applicable Creative Commons License

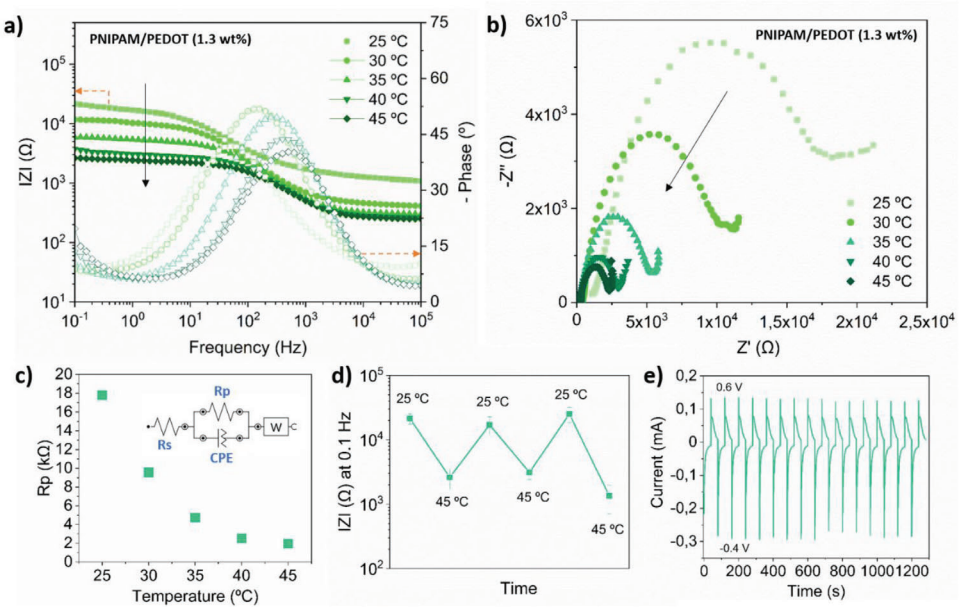

Figure 4. a) Bode Plot and b) Nyquist Plot of PNIPAM/PEDOT (1.3 wt.%) hydrogel at different temperatures obtained by EIS using PBS as the electrolyte, Pt wire as the counter electrode and Ag/AgCl electrode as the reference electrode. c) Resistance of PNIPAM/PEDOT (1.3 wt.%) hydrogel at different temperatures extracted from the equivalent circuit fit, d) Impedance magnitude at 0.1 Hz for the PNIPAM/PEDOT (1.3 wt.%) hydrogel during three temperature cycles between 25 and 45 °C and e) Chronoamperometry measurement performed to PNIPAM/PEDOT (1.3 wt.%) hydrogel by applying repetitive pulses at −0.4 and 0.6 V (versus Ag/AgCl) for 1300 s.

results demonstrate that incorporating PEDOT:PSS into the gel matrix imbues it with electrochemical sensitivity to temperature fluctuations in the electrolyte, adding a novel dimension of the material response beyond the purely physical changes exhibited by PNIPAM alone.

To quantify these changes, EIS spectra with two electrical circuit models was fitted. The Nyquist Plot can be successfully fitted ($x^2 < 1$); in the case of pristine PEDOT:PSS control, a Randles circuit with a constant phase element (CPE) in series was utilized (Figure S15a, Supporting Information). In the case of PNIPAM/PEDOT hydrogel samples, a Randles circuit involving a Warburg diffusion impedance (W) in series and a constant phase element (CPE) replacing the capacitance was used (Figure S15b, Supporting Information and see the inset of Figure 4c).[85,86] The resistor (Rs) in series represents electrolyte resistance, while the resistor (Rp) and capacitor (C or the CPE) correspond to the charge transfer resistance and double-layer capacitance created at the electrolyte-electrode interface of the hydrogels, respectively. The Warburg element (W) in the hydrogel circuit refers to the impedance arising from the diffusion of the ions. The different fitting circuits of pristine PEDOT:PSS and PNIPAM/PEDOT hydrogels can be explained by the fact that pristine PEDOT:PSS is 2D and PNIPAM/PEDOT hydrogels have a 3D structure. The values obtained for each circuit element fitted are summarized in Table S1 (Supporting Information).

First, the impedance characteristics of the PNIPAM/PEDOT hydrogels at a constant temperature were compared. For example, at 35 °C, as the PEDOT:PSS concentration increases in the hydrogel matrix, the charge transfer resistance decreases from 4370 to 42 kΩ and 4 kΩ for PNIPAM/PEDOT (0, 0.5 and 1.3 wt.%) hydrogels, respectively. The PNIPAM/PEDOT (1.3 wt.%) is the most conducting hydrogel, however, it still has higher resistance than pristine PEDOT:PSS film (0.05 kΩ) control due to the presence of insulating PNIPAM in the matrix.

Next, the change in impedance properties with temperature was quantified. When the temperature increases from 25 to 45 °C, the resistance of the samples decreases by 26.5%, 30.0%, 77.5%, and 89.0% for pristine PEDOT:PSS film and PNIPAM/PEDOT (0, 0.5 and 1.3 wt.%) hydrogels, respectively (Table S1, Supporting Information). The C or CPE values related to the capability to store the charge remain almost constant with temperature since the number of PEDOT:PSS in each sample does not change with temperature fluctuations. However, the charge transfer resistance decreases, indicating that the electrostatic coupling of cations with PEDOT:PSS becomes easier or faster with the temperature increase, thanks to the well-connected PEDOT:PSS chains when the material is shrunk. It is well noted that the swelling percentage of PNIPAM/PEDOT (0.5 wt.%) hydrogel is higher than that of PNIPAM/PEDOT (1.3 wt.%) hydrogel (Figure 3b), thus expecting a larger resistance change in the PNIPAM/PEDOT (0.5 wt.%) hydrogel with temperature. However, the difference in conductivity between both samples makes the PNIPAM/PEDOT (1.3 wt.%) hydrogel have the most significant resistance change with temperature, as well as the best conductivity, although it has the lowest swelling ratio.

To determine if the temperature-induced conductivity change is reversible, the temperature was ramped up and down for PNIPAM/PEDOT (1.3 wt.%) hydrogel. Figure 4d shows that impedance magnitude at 0.1 Hz is stable after three temperature cycles between 25 and 45 °C. In addition, the electrical stability of the PNIPAM/PEDOT (1.3 wt.%) hydrogel was analyzed by EIS over time. Figure S16 (Supporting Information) shows the Bode Plot of the material at the beginning of the experiment and after one week of immersion in PBS solution, showing a

© 2024 The Authors. Advanced Functional Materials published by Wiley-VCH GmbH

16163028, 2024, 40, Downloaded from https://onlinelibrary.wiley.com/doi/10.1002/adfm.202403708 by Universidad Del Pais Vasco, Wiley Online Library on [08/10/2024]. See the Terms and Conditions (https://onlinelibrary.wiley.com/terms-and-conditions) on Wiley Online Library for rules of use; OA articles are governed by the applicable Creative Commons License

good electrical stability over time. This result suggests the suitability of the PNIPAM/PEDOT (1.3 wt.%) hydrogel for human temperature monitoring where long-term stability and thermo-responsivity of the material are of great importance. Figure 4e shows the stability of PNIPAM/PEDOT (1.3 wt.%) hydrogel under repetitive voltage pulses at −0.4 and 0.6 V (versus Ag/AgCl) applied for ca. 20 min. Additionally, the cyclic voltammetry curves of different hydrogels were determined at different temperatures (25, 30, 35, 40 and 45 °C) and over 10 cycles (Figure S17a–e, Supporting Information) in a potential range of −0.4 to 0.6 V versus Ag/AgCl at 20 mV s^{-1}, showing good electrochemical stability. Overall, PNIPAM/PEDOT (1.3 wt.%) hydrogel has the lowest impedance values and the greatest change in conductivity with temperature, along with high thermal and electrochemical stability. Thus, this hydrogel composition was selected for further integration in OECTs to develop multifunctional thermo-responsive devices.

2.4. Fabrication and Characterization of a Thermo-Responsive OECT

A schematic representation of the thermo-responsive OECT is presented in **Figure 5a**. This transistor involves a PEDOT:PSS thin film channel, patterned between two Au electrodes, source and drain. A flow of charge carriers is created with a bias voltage (V_{DS}) applied between these two electrodes, monitored as the source-drain current (I_{DS}). This channel current can be tuned by applying a voltage (V_{GS}) at the gate electrode versus the source contact. The gate electrode is immersed in PBS, which covers the channel. In the absence of V_{GS}, the channel is in its conductive state, oxidized, and the application of a positive V_{GS} results in the reduction of the PEDOT:PSS, and hence, the device is switched off.

PNIPAM/PEDOT (1.3 wt.%) hydrogel was integrated into the OECT as the gate electrode because, in this configuration, the channel could be used multiple times even if the lifetime of the external gate electrode is limited.[87] As the functional gate electrode undergoes a change in its impedance, the channel current modulation is expected to vary. Notably, since the OECT acts as a transconductance amplifier, the channel current reflects an amplified change in the gate electrode characteristics triggered by temperature. Figure 5b shows an optical image of the microscale, photolithographically patterned PEDOT:PSS channel (10 × 100 µm) and the PNIPAM/PEDOT (1.3 wt.%) hydrogel-based gate electrode, which form the bases of the thermo-responsive OECT. In Figure 5c, images that evidence the contraction of the gate electrode upon an increase in temperature are shown, which directly modulates the channel current. It can be appreciated in the OECT sensor operation that the gel-coated gate electrode is continuously immersed in substantial volume of electrolyte (200 µL of PBS), alongside the OECT channel.

Figure 5d and e show the transfer curves of the same channels gated by either a pristine PEDOT:PSS gate (used as control) or the PNIPAM/PEDOT (1.3 wt.%) hydrogel gate at different temperatures (25, 30, 35, 40 and 45 °C) (see Figures S18 and S19, Supporting Information for the output curves obtained at each temperature). The pristine PEDOT:PSS thin film gated channels show no change in their current output as well as transconductance values (Figure S20a, Supporting Information) to changes in PBS temperature. On the contrary, the devices gated with PNIPAM/PEDOT (1.3 wt.%) hydrogel undergo significant changes (Figure S20b, Supporting Information). The OECT gated with PNIPAM/PEDOT (1.3 wt.%) hydrogel exhibits not only higher I_{DS} with an increase in temperature, but also clear changes in transconductance profile. The maximum transconductance (g_m) increases from 11.4 ± 0.4 mS at 25 °C to 13.1 ± 0.3 mS at 45 °C, and, with a shift in its position from V_{GS} = −0.3 V to V_{GS} = −0.15 V (Figure S20b, Supporting Information). This change in OECT performance can be explained by the fact that the charge transfer resistance of PNIPAM/PEDOT (1.3 wt.%) hydrogel decreases with temperature due to shrinkage.

To use the developed PEDOT:PSS OECT with PNIPAM/PEDOT (1.3 wt.%) hydrogel gate as thermo-responsive device for human temperature monitoring, a calibration curve was plot using Equation 4, with I_D values at V_D = −0.6 V and V_G = 0 V obtained at different temperatures. Figure 5f shows that the normalized response (NR) of the PNIPAM/PEDOT (1.3 wt.%) hydrogel-gated device follows almost a linear relationship with temperature and increases up to 1.12 ± 0.24 at 45 °C, compared to the very low NR values of the pristine PEDOT:PSS gated devices (NR at 45 °C = 0.06 ± 0.05). The device has not only excellent sensitivity (0.05 $°C^{-1}$) to temperature, but its temperature-induced-output is reproducible. Figure 5g shows that the I_D is around the same values each time the temperature is ramped up and down between 25 and 45 °C. These results suggest that the developed thermo-responsive OECT is a promising device for human long-term temperature monitoring applications.

2.5. In Vitro Insulin-FITC Drug Delivery using an OECT

Recent studies have highlighted the primary use of PNIPAM-based hydrogels in reversible drug delivery, attributed to PNIPAM's phase transition near human body temperature.[37,38] In the same vein, we aim to demonstrate the potential of this thermo-responsive hydrogel in drug delivery, leading to the development of a multifunctional OECT-based hydrogels. As the PEDOT:PSS channel of the OECT has been demonstrated to be used as glucose sensor,[88] Insulin-FITC was selected as the molecule for drug delivery related to chronic diabetes. In addition, the integration of this thermo-responsive OECT sensors with insulin delivery system can be advantageous to leverage the interplay between temperature fluctuation, glucose level, and insulin delivery processes. **Figure 6a** depicts the PNIPAM's general mechanism for drug delivery, where the PNIPAM/PEDOT (1.3 wt.%) hydrogel undergoes a reversible phase transition in an aqueous solution from hydrophilic state to hydrophobic state around its LCST at 35 °C. Below this LCST, the hydrogel absorbs Insulin-FITC, and above it, the hydrogel releases drug. The process of drug loading into the PNIPAM/PEDOT (1.3 wt.%) hydrogel was examined through a simple swelling technique, immersing the hydrogel in a 0.1 mg mL^{-1} Insulin-FITC solution (in PBS) for 24 h. The reduction in fluorescent intensity of the supernatant post-immersion, as shown in Figure S21 (Supporting Information), confirms successful drug incorporation into the hydrogels.

© 2024 The Authors. Advanced Functional Materials published by Wiley-VCH GmbH

16163028, 2024, 40, Downloaded from https://onlinelibrary.wiley.com/doi/10.1002/adfm.202403708 by Universidad Del Pais Vasco, Wiley Online Library on [08/10/2024]. See the Terms and Conditions (https://onlinelibrary.wiley.com/terms-and-conditions) on Wiley Online Library for rules of use; OA articles are governed by the applicable Creative Commons License

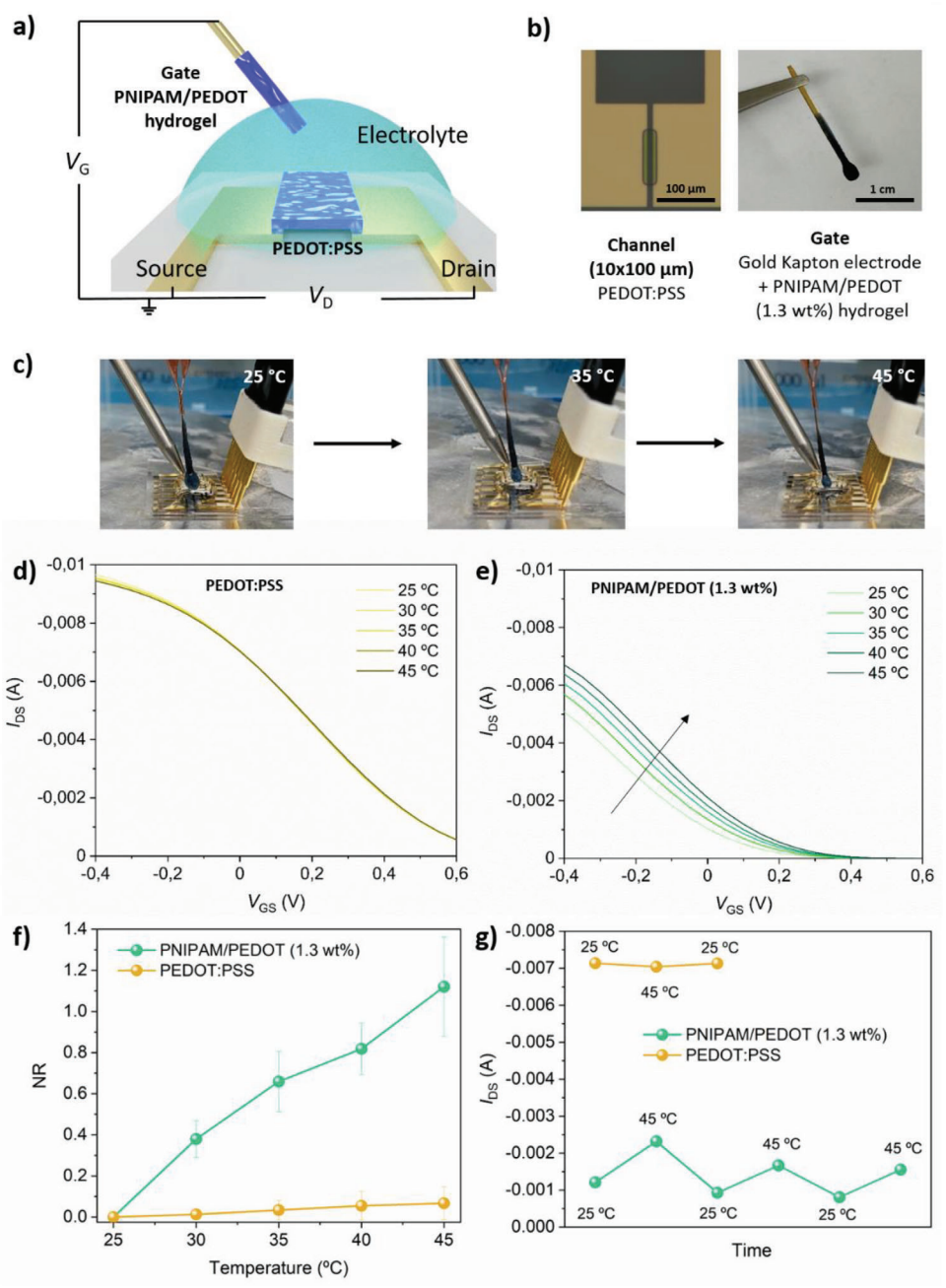

Figure 5. a) A schematic representation of the OECT with PEDOT:PSS channel and PNIPAM/PEDOT (1.3 wt.%) hydrogel gate immersed in PBS. b) Pictures of the PEDOT:PSS channel (10 µm in length x 100 µm in width) and the PNIPAM/PEDOT (1.3 wt.%) hydrogel based gate electrode. c) Pictures of the characterization set up and PNIPAM/PEDOT (1.3 wt.%) hydrogel gate contraction with a temperature increase from 25 °C, to 35 °C and 45 °C. The transfer curves at different temperatures obtained for PEDOT:PSS channels gated with a d) PEDOT:PSS thin film coated Au electrode and e) PNIPAM/PEDOT (1.3 wt.%) hydrogel gate (V_D = −0.6 V). f) Normalized response (NR) of the control and temperature-responsive OECTs as a function of temperature (V_D = −0.6 V and V_G = 0 V) and g) The channel current values of temperature-responsive OECT obtained during three temperature cycles between 25 and 45 °C (V_D = −0.6 V and V_G = 0 V).

FTIR analysis was performed on various samples to confirm the encapsulation of Insulin-FITC within the PNIPAM/PEDOT (1.3 wt.%) hydrogel, as shown in Figure S22 (Supporting Information). The FTIR spectra reveal characteristic signals for secondary amides and carboxylic acids (functional groups of amino acids in the protein) which are absent in the drug-free hydrogel. The peaks at ≈3450 cm^{-1} (N-H stretching vibration), 1495 cm^{-1} (N-H bending vibration), 1250 cm^{-1} (C-N and O-C-C stretching vibration), and 900 cm^{-1} (O-H bending vibration) corroborate the successful drug loading. Subsequent analysis focused on the release kinetic of Insulin-FITC at 25 and 37 °C, simulating ambient and human body conditions, respectively. The

© 2024 The Authors. Advanced Functional Materials published by Wiley-VCH GmbH

16163028, 2024, 40, Downloaded from https://onlinelibrary.wiley.com/doi/10.1002/adfm.202403708 by Universidad Del Pais Vasco, Wiley Online Library on [08/10/2024]. See the Terms and Conditions (https://onlinelibrary.wiley.com/terms-and-conditions) on Wiley Online Library for rules of use; OA articles are governed by the applicable Creative Commons License

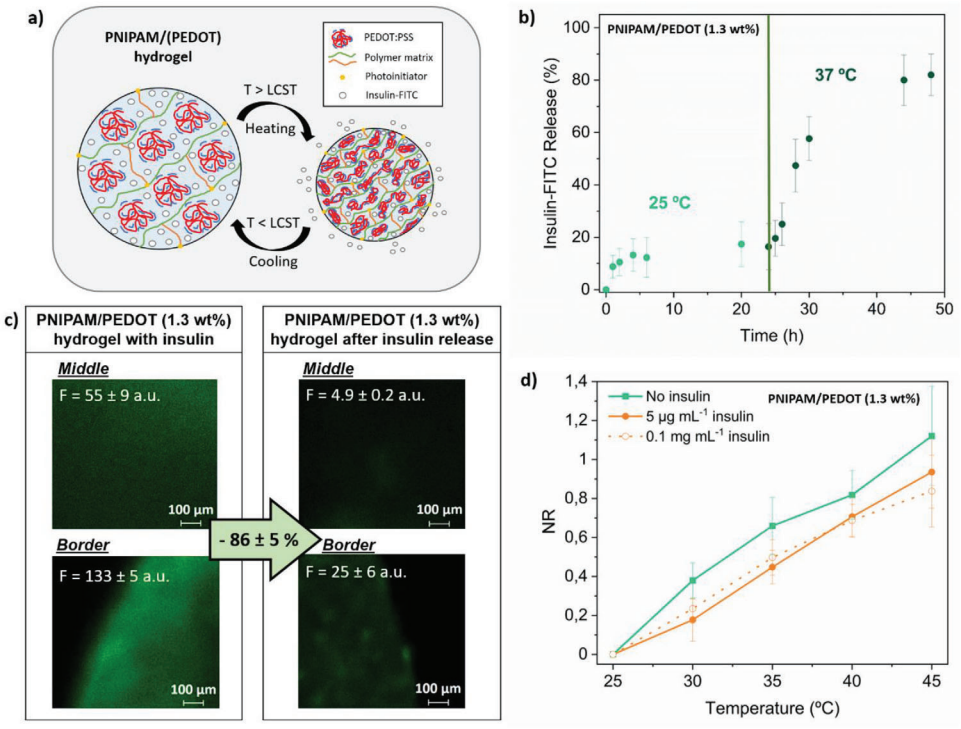

Figure 6. a) PNIPAM/(PEDOT) hydrogel general mechanism for drug delivery. b) In vitro accumulated Insulin-FITC release (%) from PNIPAM/PEDOT (1.3 wt.%) hydrogel at 25 and 37 °C in PBS solution for 24 h each (the % of drug released was measured analyzing fluorescence emission of the supernatant). c) Fluorescence intensity of confocal microscope images of the middle and border parts of the PNIPAM/PEDOT (1.3 wt.%) hydrogel before and after Insulin-FITC release at 37 °C. d) Normal response (NR) of the PEDOT:PSS OECT using PNIPAM/PEDOT (1.3 wt.%) hydrogel gate swollen in PBS solution, 5 µg mL^{-1} Insulin-FITC solution and 0.1 mg mL^{-1} Insulin-FITC solution versus temperature ($V_D = -0.6$ V and $V_G = 0$ V).

release profile was monitored via fluorescence spectroscopy over time and compared to a calibration curve of standard insulin solutions with known concentrations (Figure S23, Supporting Information).[89] At room temperature, the hydrogels demonstrates a release plateau of 20 ± 5% within 5 h, indicative of a diffusion-driven release mechanism (Figure 6b). Conversely, at 37 °C, i.e., above the PNIPAM/PEDOT (1.3 wt.%) hydrogel's LCST, the drug release escalates up to a stable value of 82 ± 4% after 24 h, highlighting the temperature-responsive behavior of the hydrogel that can speed up the drug release. In addition, Figure 6c shows the fluorescence intensity of confocal microscope images of the middle and border parts of the PNIPAM/PEDOT (1.3 wt.%) hydrogel before and after drug release at 37 °C. In this way, the released Insulin-FITC from the hydrogel can be quantified, losing almost the 86 ± 5% of drug, a comparable result with the data obtained by fluorescence spectroscopy. Finally, the FTIR of the hydrogel after drug release was also analyzed to confirm the absence of Insulin-FITC in the sample (Figure S22, Supporting Information), where it cannot be found any peak related to the insulin molecule.

To evaluate the effect of Insulin-FITC on the thermo-responsivity and functionality of the hydrogel-gated OECT device, the NR of the OECT was assessed over time with the PNIPAM/PEDOT (1.3 wt.%) hydrogel gate infused with Insulin-FITC solutions at concentration of 5 µg mL^{-1} and 0.1 mg mL^{-1} (Figure 6d). The findings indicate the insulin presence within the hydrogel gate does not significantly impact the OECT's NR across varying temperatures, with observed variations lying within the standard deviation range. This suggest that insulin incorporation does not alter the OECT's operational efficiency. Further analysis involved examining the transfer curve and transconductance (Figure S24a,b, Supporting Information respectively) of a PEDOT:PSS OECT, using different concentrations of Insulin-FITC (ranging from pg mL^{-1} to mg mL^{-1} range) in PBS solution as the electrolyte and standard Ag/AgCl electrode as the gate electrode. These tests demonstrate that insulin presence within PBS electrolyte does not influence the OECT's performance, confirming this device suitability for integrated long-term temperature monitoring and insulin drug delivery applications.

3. Conclusion

In conclusion, multifunctional thermo-responsive and conductive PNIPAM/PEDOT hydrogels have been successfully processed by Digital Light Processing (DLP) 4D printing. Initially, NIPAM/PEDOT:PSS inks were optimized which show ideal characteristics as fast photopolymerization kinetics and low viscosity values in order to obtain high-resolution (100 µm) 4D printed hydrogels. Interestingly, these PNIPAM/PEDOT hydrogels undergo a reversible phase change from hydrophilic state to hydrophobic state at their low critical solution temperature (LCST), ≈35 °C. Results reveal that hydrogels not only exhibit deswelling and shrinkage above their LCST, but also, they become stiffer with temperature increase due to water release from the polymer

© 2024 The Authors. Advanced Functional Materials published by Wiley-VCH GmbH

16163028, 2024, 40, Downloaded from https://onlinelibrary.wiley.com/doi/10.1002/adfm.202403708 by Universidad Del Pais Vasco, Wiley Online Library on [08/10/2024]. See the Terms and Conditions (https://onlinelibrary.wiley.com/terms-and-conditions) on Wiley Online Library for rules of use; OA articles are governed by the applicable Creative Commons License

matrix, presenting a Young's Modulus of 0.19 ± 0.04 MPa at 25 °C and 0.46 ± 0.04 MPa at 45 °C. In addition, PNIPAM/PEDOT hydrogels show neither chemical nor thermal degradation and they are biocompatible with murine myoblast cells (C_2C_{12}) according to the performed LIVE/DEAD assay, being able to be integrated in biomedical devices for long-term monitoring applications. Electrochemical characterization shows that PNIPAM/PEDOT (1.3 wt.%) hydrogel charge transfer resistance decreases a 89.0% with temperature increase from 25 to 45 °C. This indicates that the redox mechanism of PEDOT:PSS becomes easier or faster with the temperature increase, probably due to the close environment in PEDOT:PSS domains when the material is shrunk.

As an application, the PNIPAM/PEDOT (1.3 wt.%) hydrogel was integrated as the gate electrode in a PEDOT:PSS OECT, showing a normal response (NR) of 1.12 ± 0.24 at 45 °C, demonstrating the great sensitivity (0.05 $°C^{-1}$) of the developed OECT to temperature fluctuations. Moreover, the developed OECT shows a reversible response with temperature, allowing their application as thermo-responsive devices for long-term human temperature monitoring. As the PEDOT:PSS channel of the OECT can act as glucose sensor, Insulin-FITC was released from the PNIPAM/PEDOT (1.3 wt.%) hydrogel gate in order to use the device in humans with chronic diabetes. Results reveal that at human body conditions, i.e., 37 °C, the hydrogel is able to release 82 ± 4% of the total amount of the initially loaded drug. In addition, the presence of Insulin-FITC in the gate or in the electrolyte does not affect the thermo-responsivity and performance of the developed OECT. As future perspective, the high printing resolution of this thermo-responsive material (≈100 µm) can be advantageous in order to alter the surface area of the gate electrode, which can affect the OECT performance, and even for its usage in smaller bioelectronic devices.[90,91]

To conclude, the newly developed multifunctional OECT is suitable for long-term temperature monitoring and insulin drug delivery system, thus leveraging the interplay between temperature fluctuation, glucose level, and insulin delivery processes. In this way, the incorporation of such multifunctional hydrogels in OECTs signifies a leap forward in the development of bioelectronic devices, poised to revolutionize healthcare diagnostics and disease treatment.

4. Experimental Section

Materials: N-isopropylacrylamide (NIPAM, > 99%), poly(ethylene glycol) diacrylate (PEGDA, average M_n 700 Da), 2-hydroxy-2-methylpropiophenone (Darocur 1173, 97%), Vitamin B2 Riboflavin (Rf), Insulin-FITC (labeled human) and phosphate buffered saline (PBS) tablets were purchased from Sigma Aldrich. PEDOT:PSS (PH1000) was received from Heraeus. The Ag/AgCl and the Pt wire electrodes were purchased from BAS Inc. (ALS-Japan). All aqueous solutions were prepared with ultrapure water (Milli-Q, Millipore). All chemicals were used without any further purification.

Pre-Polymeric Mixture Preparation: Various inks were prepared employing different concentrations of PEDOT:PSS. For this purpose, PEDOT:PSS aqueous solutions of different concentrations (0, 0.5 and 1.3 wt.%) were prepared, using only water in the case of the 0 wt.% one, or diluting the commercial PH1000 solution to the half in the case of 0.5 wt.% one. Subsequently, the NIPAM monomer (45 wt.% of the total ink composition) was dissolved in previously prepared PEDOT:PSS aqueous solutions (50 wt% of the total ink composition). Then, PEGDA crosslinker and Darocur/Rf (10 mg mL^{-1} aqueous solution) (1/1) photoinitiator mixture were added in a 3 wt.% and 2 wt.% amount, respectively, with respect to the total ink composition. Finally, the inks were sonicated at 30 °C for 15 min to obtain a homogeneous solution.

Hydrogel Synthesis: PNIPAM/PEDOT hydrogels were synthesized employing previously described pre-polymeric mixtures, where the concentration of PEDOT:PSS changed. The inks were sonicated for 15 min and irradiated with UV light to induce photopolymerization in silicone molds of various dimensions at 25 °C.

PNIPAM Synthesis: PNIPAM was synthesized by free radical polymerization as follows: 1 g of NIPAM was dissolved in a round bottom flask containing 100 mL of toluene. To this solution, 0.05 g of azobisisobutyronitrile (AIBN) thermal initiator was added. The solution was bubbled with N_2 for 30 min in order to remove the oxygen, and heated at 75 °C for 2 days. The polymer was purified by precipitation in diethyl ether. A yield of 53% was obtained. [^{1}H-NMR (500 MHz, DMSO-d_6) δ 7.58 – 6.99 (m, 1H), 3.85 (s, 1H), 2.03 (m, 1H), 1.72 – 1.15 (m, 2H), 1.16 – 0.92 (m, 6H)]. GPC (M_n = 21 450 g mol^{-1}, M_w = 43 622 g mol^{-1}, PD = 2.03).

Kinetic Measurements by FTIR: The photopolymerization reaction kinetics were studied by Fourier Transform Infrared Spectroscopy (FTIR). FTIR spectra of previously described inks were recorded in the Attenuated Total Reflectance (ATR) mode in a Thermo Scientific model Nicolet 6700 FTIR spectrometer, with a resolution of 4 cm^{-1}, mirror speed of 0.3165, and 5 scans. Pre-polymeric mixtures were placed in a zinc selenide glass, and ATR-FTIR spectra were recorded at room temperature every 0.1 min by exposing the photocurable inks to UV light (wavelength = 390 ± 20 nm, power = 2 mW cm^{-2}) for 5 min. The conversion was calculated with Equation 1 by measuring the area of the peaks located at 955 and 985 cm^{-1}, which correspond to the C═C out-of-plane bending vibration:

$$Conversion\ (\%) = \left(1 - \frac{A_t}{A_0}\right) \times 100 \quad (1)$$

where A_t is the area of the band at a time t, and A_0 is the area of the band at zero time.

Viscosity Measurements: Viscosity measurements of inks containing 0, 0.5 and 1.3 wt.% PEDOT:PSS were carried out in an Anton Paar rheometer at room temperature using concentric cylinders (CC17 17 488 model). The viscosity of the inks was studied from 1000 to 0.1 s^{-1} shear rate values.

3D printing: PNIPAM/PEDOT 1.3 wt.% ink was placed into the vat of the 3D printer (Anycubic Photon Mono X 6K) and exposed to light irradiation (wavelength = 405 nm, power = 2 mW cm^{-2}). A layer height of 0.1 mm and exposure time of 30 s were applied as the printing conditions. In order to determine the resolution of the material, a standard model with holes of 1000, 500, 250 and 100 µm, a 500 µm hole size scaffold and a flower were designed with Autodesk Inventor 2022 software. These objects were printed. Afterward, the printed structures were washed gently with Milli-Q water.

Rheology: Dynamic Mechanical Analysis (DMA) and Dynamic Mechanical Thermal Analysis (DMTA) were performed using a TA Instruments DMA Q800 apparatus. Photopolymerized PNIPAM/PEDOT hydrogels containing 0, 0.5 and 1.3 wt.% of PEDOT:PSS were cut in a rectangular shape of 2 cm x 1 cm for the measurements. For DMA, scans of all samples were conducted from 0.01 to 35 Hz at 25 °C on bending mode. For DMTA, only PNIPAM/PEDOT 1.3 wt.% hydrogel was tested in compression mode, scanning the sample at a frequency of 1 Hz from 0 to 200 °C, at 10 °C min^{-1}.

Differential Scanning Microcalorimetry (micro-DSC): PNIPAM/PEDOT hydrogels, PNIPAM polymer and PEDOT:PSS aqueous solution were analyzed in a MicroCalvet VII microcalorimeter from Setaram equipped with a Julabo F-32 thermostatic bath. All the samples were placed into Hastelloy C276 hermetic cells (total volume of 1 cm^3) containing wet hydrogel discs (25-30 mg) and ≈400 µL Milli-Q water; reference was set with ≈400 µL Milli-Q water. In the case of PNIPAM polymer and PEDOT:PSS solution, at least 300 mg were placed into the sample cell; and a similar mass of Milli-Q water was placed into the reference cell. Non-isothermal experiments were conducted at 0.2, 0.5 and 1 °C min^{-1} for the determination of the LCST; sequential heating and cooling steps were performed from −10 to 65 °C (30 °C above the LCST) in order to evaluate the reversibility of

© 2024 The Authors. Advanced Functional Materials published by Wiley-VCH GmbH

16163028, 2024, 40, Downloaded from https://onlinelibrary.wiley.com/doi/10.1002/adfm.202403708 by Universidad Del Pais Vasco, Wiley Online Library on [08/10/2024]. See the Terms and Conditions (https://onlinelibrary.wiley.com/terms-and-conditions) on Wiley Online Library for rules of use; OA articles are governed by the applicable Creative Commons License

the process through the determination of the enthalpies; PNIPAM polymer and PEDOT:PSS solutions were tested from 0 to 80 °C at the same heating/cooling rates. In order to determine the enthalpy values correctly, the swelling factor of the hydrogels was taken into consideration.

Swelling Test: Discs of PNIPAM/PEDOT hydrogels (1 mm thickness and 1 cm diameter) were prepared, cleaned in distilled water, and weighed (W_0) once totally dried. Subsequently, they were immersed in a PBS solution at 25 °C for 1 day. The PBS solution was heated slowly, and at established temperatures (every 1.5 °C, from 25 to 45 °C), the samples were removed from the PBS solution, and externally dried with filter paper to eliminate the excess of water that could remain on the surface, and weighed (W_t). The swelling percentage (S_w) was calculated according to Equation 2:

$$Sw = \frac{W_t - W_0}{W_0} \times 100 \quad (2)$$

Degradation Test: PNIPAM/PEDOT hydrogels, 1 cm in diameter and 1 mm thick, were initially rinsed with distilled water. Post-cleaning, these samples were air-dried at room temperature for weight measurement. They were then immersed in a PBS solution containing (0.01 M phosphate buffer, pH = 7.4) and incubated at 37 °C. Weight assessment were conducted at 24 h, 72 h, 1 week, and 2 weeks after removal from the PBS solution and subsequent air-drying at room temperature. The weight of the dried samples was determined in order to calculate the weight loss during the time they remained in the PBS solution at 37 °C. Additionally, the changes in surface morphology was analyzed by SEM.

Contact Angle: The water contact angle for the PNIPAM/PEDOT (1.3 wt.%) hydrogel was measured using an OCA 20 Instrument (Data Physics), when the hydrogel was removed from the PBS solution at 25 and 45 °C. The measurement of the contact angle was done by placing a 10 µL droplet of distilled water on the hydrogel surface. The given values, which were recorded 2 s after the deposition of the water droplet on the surface of the sample, are an average of 10 measurements per hydrogel.

Tensile Test: The PNIPAM/PEDOT (1.3 wt.%) hydrogel underwent tensile testing using Type V probe-shaped samples, as per ASTM D638. The tensile tests were performed on samples immersed in PBS solution at 25, 35 and 45 °C for 1 day using an Instron 5569 in a single uniaxial tensile mode (n = 5). The controlled tension force (load cell of 100 N) was applied at a rate of 1 mm min^{-1}, and the results were plotted as stress–strain curves.

Thermogravimetric Analysis (TGA): In order to determine the thermal stability of each sample, the thermogravimetric analysis was carried out on a TGA Q500 (TA Instruments) equipment, with a heating rate of 10 °C min^{-1} from 40 to 800 °C under N_2 atmosphere.

Scanning Electron Microscopy (SEM): SEM analysis was conducted using a Hitachi Tabletop Microscope (TM3030 series) at a 15 kV force field, running in a point-by-point scanning mode. The printed samples were placed on an aluminum holder with double-sided carbon tape and introduced into the SEM chamber. The SEM images were analyzed using ImageJ software.

Atomic Force Microscopy (AFM): The surface topology of PNIPAM/PEDOT (1.3 wt.%) hydrogel was characterized by AFM (Bruker Dimension Icon, Germany) in tapping mode. The temperature of the AFM plate was incrementally increased from 25 to 45 °C in 5 °C steps. Nanoscope Analysis software was employed for the visualization and analysis of the AFM images. As for the sample preparation, the hydrogel was directly photopolymerized on the aluminium substrate and heated in the AFM plate.

Nuclear Magnetic Resonance Spectroscopy (NMR): ^{1}H-NMR spectrum of PNIPAM polymer was recorded with a Bruker Avance NEO 500 (Probe BBOF Gradient in GZ) at 500 MHz resonance frequency at room temperature. The sample was dissolved in CD_3SOCD_3 solvent in order to make the analysis. As for the final spectrum, it was referenced to solvent peaks with chemical shifts reported in ppm.

Gel Permeation Chromatography (GPC): The molecular weight of PNIPAM polymer was determined by GPC. It was dissolved in GPC grade THF at a concentration of roughly 1 mg mL^{-1}. Then, it was filtered (polyamide Φ = 45 µm) before being injected into the GPC via an auto sampler (Waters 717, Milford, MA). A pump (LC-20A; Shimadzu, Japan) controlled a THF flow of 1 mL min^{-1}. The GPC was composed of a differential refractometer (Waters 2410, Milford, MA) and three columns in series (Styragel HR2, HR4, and HR6, with pore sizes ranging from 102 to 106 Å). Measurements were performed at 35 °C. Molecular weights were determined using a calibration curve based on polystyrene standards.

LIVE/DEAD assay: The International Organization for Standardization, ISO 10993–5, requires biological testing of medical devices or materials used in medical devices through a cytotoxicity assay.[70] Following these requirements, a general assessment of the cytotoxicity and biocompatibility of the PNIPAM/PEDOT hydrogels was done through a LIVE/DEAD assay. The different hydrogels were carefully placed in a Falcon 48-well plate (Corning) and a smaller well was placed around them to prevent the hydrogel from floating in the media. Murine myoblast cells, C_2C_{12}, (6000 cells cm^{-2}, P.7) were seeded on the PNIPAM/PEDOT hydrogels and on the plate, polystyrene, as a positive control. After 24 h of culture, cells were incubated with 3 µm Calcein AM (Sigma–Aldrich) and 3.5 µm PI (Sigma–Aldrich) in PBS containing Ca^{2+} and Mg^{2+} (Gibco), for 15 min at 37 °C and fluorescent images were captured using a 10X objective in an inverted Leica DMi8 microscope (Leica). Calcein AM is converted to a fluorescent molecule, green, when it interacts with viable cells; on the contrary, PI, which reacts with the nuclei content of dead cells, generates a red signal. Cell viability was calculated counting the live and dead cells in each hydrogel using ImageJ software. The cell viability was normalized with respect to the polystyrene positive control. Additionally, cell confluence (%) in the PNIPAM/PEDOT hydrogels was quantified based on the ratio of the cultured cells covering the adhesion surface of the substrates.

Lactate Dehydrogenase (LDH) Assay: Following the procedures indicated by ISO 10993-12[92] to generate sample extracts, PNIPAM/PEDOT (0, 0.5 and 1.3 wt.%) hydrogels were incubated with cell culture media for 48 h at 37 °C. C_2C_{12} cells were seeded at a density of 5.0×10^3 cells ml^{-1} on a 96-well plate. As cells reached ≈80% confluence, their media was exchanged with the media that was previously incubated with the PNIPAM/PEDOT hydrogels to have contact with extracts of the substrates. After 24 h of incubation, the release of LDH by cells, as a measure of cytotoxicity, was assessed using a CytoTox 96 Non-Radioactive Cytotoxicity Assay (Promega) and following the manufacturer's protocol. Briefly, 50 µL of media from all tests and control wells were transferred to a new 96-well plate. Then 50 µL CytoTox 96 reagent were added and mixed to each of the wells containing sample and incubated at room temperature and in the dark for 30 min on a gentle rocker. 50 µL of stop solution included in the kit were added to each well and absorbance was measure at 490 nm. The maximum LDH release is the amount of enzyme released by lysed cells, as a negative control. The cytotoxicity percentage was found using Equation 3.

$$Percent\ cytotoxicity = \left(\frac{Experimental\ LDH\ Release\ (OD_{490})}{Maximum\ LDH\ Release\ (OD_{490})}\right) \times 100 \quad (3)$$

Cell Culture: Murine myoblast cells, C_2C_{12} (Thermofisher Scientific) were routinely maintained in Dulbecco's Modified Eagle's Media, DMEM (Gibco), complemented with 20% fetal bovine serum, FBS (Gibco), and 1% penicillin–streptomycin, P/S (Gibco). All cultures were maintained in a humidified incubator, 37 °C and 5% CO_2.

Electrode Preparation: The electrode substrate was a Kapton (polyimide) film with a thickness of 175 µm. The Kapton was cut with a Silhouette cutting machine into a square geometry that defined the electrode active area (2×2 mm^2). Then, a 10 nm of Cr and 100 nm of Au was sputtered onto the cleaned substrates. Prior to the hydrogel coating, the gold kapton electrodes were treated with a 3-mercaptopropyltrimethoxysilane (MPTMS) 10 mM solution in isopropyl alcohol and distilled water (3:1 ratio) for 1 min, followed by isopropanol cleaning. Then, the electrodes underwent drying and activation using O_2 plasma (25 Watt, 1 min).

PEDOT:PSS electrode, serving as a control sample, was prepared in the following way; the aqueous dispersion of PEDOT:PSS PH1000 containing ethylene glycol (5 vol.%), sodium dodecylbenzenesulfonate (0.25 vol.%), and (3-glycidyloxypropyl)trimethoxysilane (1 wt.%) was sonicated and

© 2024 The Authors. Advanced Functional Materials published by Wiley-VCH GmbH

16163028, 2024, 40, Downloaded from https://onlinelibrary.wiley.com/doi/10.1002/adfm.202403708 by Universidad Del Pais Vasco, Wiley Online Library on [08/10/2024]. See the Terms and Conditions (https://onlinelibrary.wiley.com/terms-and-conditions) on Wiley Online Library for rules of use; OA articles are governed by the applicable Creative Commons License

16163028, 2024, 40, Downloaded from https://onlinelibrary.wiley.com/doi/10.1002/adfm.202403708 by Universidad Del Pais Vasco, Wiley Online Library on [08/10/2024]. See the Terms and Conditions (https://onlinelibrary.wiley.com/terms-and-conditions) on Wiley Online Library for rules of use; OA articles are governed by the applicable Creative Commons License

10 µL of the solution were drop-casted in the gold kapton electrode followed by an annealing at 140 °C for 30 min. Whereas, different PNIPAM/PEDOT hydrogel electrodes (0, 0.5 and 1.3 wt.%) were similarly prepared, involving 10 µL ink deposition onto the gold kapton electrode, followed by a photopolymerization step with UV light irradiation. Finally, all the samples were cleaned in a PBS solution for 1 day. In the case of the PNIPAM/PEDOT hydrogel electrodes, they were stored in the PBS solution to avoid water evaporation.

Electrochemical Measurements: Electrochemical impedance spectroscopy (EIS) was employed to measure the resistivity of PNIPAM/PEDOT hydrogels using an Autolab 302 N potentiostat galvanostat. Measurements were taken across a range of temperatures (25 to 45 °C) using a three-electrode setup with Pt wire as the counter electrode, Ag/AgCl electrode as the reference electrode, and the prepared PNIPAM/PEDOT hydrogel electrodes as the working electrode. PBS aqueous solution was used as the electrolyte, and EIS data, including Bode and Nyquist plots, were acquired across a frequency range of 0.1 Hz to 100 kHz with 10 mV amplitude perturbation at open circuit potential (OCP) conditions. The reversibility of PNIPAM/PEDOT (1.3 wt.%) hydrogel was analyzed by measuring the EIS for 3 temperature cycles, at 25 and 45 °C. The EIS fitting analysis was carried out using the NOVA software. In addition, the electrical stability of PNIPAM/PEDOT (1.3 wt.%) hydrogel was analyzed by EIS over time after one week of the material immersion in a PBS solution. Besides, a chronoamperometry measurement was performed to PNIPAM/PEDOT (1.3 wt.%) hydrogel by applying repetitive pulse potentials of −0.4 and 0.6 V (versus Ag/AgCl) for 1300 s, which is similar to 30 cycles. Finally, cyclic voltammetry (CV) was performed to PNIPAM/PEDOT hydrogels using a VMP-3 potentiostat (Biologic Science Instruments) in a three-electrode setup, employing a platinum wire as the counter electrode, Ag/AgCl as the reference electrode and PBS solution as the liquid electrolyte. Cyclic voltammetry measurements were carried out in the potential range of −0.4 to 0.6 V versus Ag/AgCl at 20 mV s^{-1} at different temperatures (25, 30, 35, 40 and 45 °C) and over 10 cycles.

OECT Fabrication: The OECTs were microfabricated on the 4-inch glass wafers using standard photolithography and parylene C peel-off techniques as described in the literature.[93–95] A first layer of photoresist (AZ5214) was spin coated and exposed to ultraviolet light using a contact aligner. The photoresist patterns were generated with AZ 726 developer, followed by metal sputtering of 10 nm Cr and 100 nm Au and a standard lift-off process using hot dimethyl sulfoxide to create electrodes and interconnection pads. Next, a second layer of photoresist AZ9260 was coated on the substrates and later developed using AZ developer. A parylene C layer was deposited to insulate the Au interconnects. The OECT channel (10 × 100 µm) was patterned by reactive ion etching, using a second layer of parylene C that could be peeled off to yield the patterns. The aqueous dispersion of PEDOT:PSS PH1000 containing ethylene glycol (5 vol.%), sodium dodecylbenzenesulfonate (0.25 vol.%), and (3-glycidyloxypropyl)trimethoxysilane (1 wt.%) was sonicated for 30 min and then spin-coated (3000 rpm.; 45 s) on the plasma-treated OECT substrates. The PEDOT:PSS OECTs were then annealed at 140 °C for 1 h to activate GOPS and avoid dissolution of the polymer film in the aqueous medium. All devices were rinsed with deionized water before use.

OECT Characterization: All measurements were conducted under ambient atmosphere conditions using a Keithley 2602A source meter unit operated by a customized LabVIEW software. The steady-state characteristics of the transistors were obtained by applying varied drain voltage (V_D) and gate voltage (V_G). The PEDOT:PSS electrode and PNIPAM/PEDOT (1.3 wt.%) hydrogel electrode were used as gate electrodes and compared their gating performance. 1xPBS was used as the electrolyte with a volume of 200 µL to cover the entire hydrogel gate. The output curves of each measurement were collected when the drain voltage (V_D) swept from 0 to −0.6 V at the increment of −0.05 V with the varied gate voltage (V_G) from −0.4 to 0.6 V at the increment of 0.1 V. The transfer curve of each measurement was constructed at $V_D = -0.6$ V along with varying V_G. For each gate, all these parameters were recorded at different temperatures (25, 30, 35, 40 and 45 °C) by placing the OECT on a hot plate and monitoring the temperature with a digital thermometer attached to the PBS electrolyte. In order to quantify the OECT response with respect to the temperature, the normalized response (NR) of the OECT using the PEDOT:PSS and PNIPAM/PEDOT (1.3 wt.%) hydrogel gate was calculated using the Equation 4:

$$NR = \frac{|I_D - I_0|}{I_0} \quad (4)$$

where I_D is the current response of the OECT at different temperatures and I_0 is the current response of the OECT at 25 °C. ($V_D = -0.6$ V and $V_G = 0$ V)

PNIPAM/PEDOT (1.3 wt.%) hydrogel's temperature sensitivity was determined by taking the slope's value of the NR versus temperature graph straight line.

In addition, reversibility of the different gates was analyzed by recording the OECT characteristics at 3 temperature cycles, between 25 and 45 °C. Moreover, the NR of the OECT was also determined when the PNIPAM/PEDOT hydrogel gate was swollen with 5 µg mL^{-1} and 0.1 mg mL^{-1} Insulin-FITC solutions in PBS. In order to check how this drug can affect the OECT performance, some experiments were carried out using some Insulin-FITC solutions of different concentrations (from pg mL^{-1} to mg mL^{-1} range) as OECT liquid electrolyte and the standard Ag/AgCl electrode as the gate. For these measurements, the gate voltage (V_G) varied from −0.2 to 0.6 V.

We assigned an OECT channel to evaluate the different gates, and the results for each gate were generated by conducting multiple measurements in this single device. To exclude any effects from the device-to-device differences, we first measured the output characteristics of each OECT channel with Ag/AgCl gate before characterizing the device with the synthetized gates. Only those devices with deviation in ON currents within 5% were further selected for the next measurements.

Insulin-FITC Loading: Insulin-FITC was loaded into PNIPAM/PEDOT (1.3 wt.%) hydrogel by a simple swelling method. The hydrogels, 1 mm thick and 1 cm in diameter, were immersed in a 0.1 mg mL^{-1} Insulin-FITC solution (in 1xPBS) for 1 day. In order to verify the drug loading of the hydrogel, fluorescence measurements of the supernatant were taken before and after 24 h hydrogel immersion. In addition, FTIR analysis were conducted on dry samples, including PNIPAM/PEDOT (1.3 wt.%) hydrogel, Insulin-FITC and PNIPAM/PEDOT (1.3 wt.%) hydrogel loaded with the drug.

Insulin-FITC Release: The temperature-dependent release of Insulin-FITC from the PNIPAM/PEDOT (1.3 wt.%) hydrogel was monitored using fluorescence spectroscopy over time in a PBS solution at 25 and 37 °C. For this purpose, the insulin-loaded hydrogels were first washed with deionized water to remove the unloaded Insulin-FITC molecules from the drug-loading step, and were placed in the PBS solution. At regular intervals, samples were withdrawn, and the fluorescence intensity of the supernatant was measured. To estimate the amount of Insulin-FITC released from the PNIPAM/PEDOT (1.3 wt.%) hydrogel at 25 and 37 °C, the Insulin-FITC released in the supernatant was determined by fluorescence spectroscopy based on comparison to a calibration curve of insulin standard solution. In addition, the FTIR of the hydrogel after drug release was analyzed to confirm the absence of Insulin-FITC in the sample. Moreover, the hydrogels before and after drug release were analyzed by confocal microscopy to quantify the Insulin-FITC loss in the samples by measuring the fluorescence intensity in the hydrogels.

Calibration Curve: A calibration curve correlating fluorescence intensity with concentration of Insulin-FITC in PBS was established. For this purpose, different Insulin-FITC standard solutions in PBS were prepared (from pg mL^{-1} to mg mL^{-1}) and measured by fluorescence spectroscopy.

Fourier Transform Infrared Spectroscopy (FTIR): FTIR spectra were recorded on a Nicolet iS20 Spectrometer using Attenuated Total Reflection (ATR) at a resolution of 2 cm^{-1} and a total of 32 interferograms. All samples were analyzed in the dry state.

Fluorescence Spectroscopy: Fluorescence measurements were performed in a Tecan Infinite M1000 Pro spectrometer monitored by Tecan i-control software. The supernatant of drug-loading and drug-release

© 2024 The Authors. Advanced Functional Materials published by Wiley-VCH GmbH

experiments, as well as calibration curve solutions were excited at λ_{exc} = 488 nm and the fluorescence emission spectra was recorded from 500 to 680 nm (λ_{max} = 516 nm).

Confocal Microscopy: A Zeiss LSM880 with Airyscan_iac microscope was used to quantify the Insulin-FITC loss during drug release experiment of PNIPAM/PEDOT (1.3 wt.%) hydrogel by measuring their fluorescence intensity (λ_{exc} = 488 nm and λ_{max} = 516 nm) before and after drug release.

Supporting Information

Supporting Information is available from the Wiley Online Library or from the author.

Acknowledgements

This work was supported by the Marie Sklodowska-Curie Research and Innovation Staff Exchanges (RISE) under grant agreement No. 823989 "ION-BIKE". Naroa Lopez-Larrea gratefully acknowledges the support from the Spanish Ministry of Universities (FPU20/03416). The authors thank Dr. Itxaso Calafel (POLYMAT, UPV/EHU) for her support regarding rheological characterization and Jessica Parrado for OECT fabrication.

Conflict of Interest

The authors declare no conflict of interest.

Data Availability Statement

The data that support the findings of this study are available from the corresponding author upon reasonable request.

Keywords

4D printing, drug delivery, hydrogels, multifunctionality, OECTs, PEDOT:PSS, PNIPAM

Received: February 29, 2024
Revised: April 16, 2024
Published online: April 26, 2024

[1] L. Bai, C. G. Elósegui, W. Li, P. Yu, J. Fei, L. Mao, *Front Chem* **2019**, *7*, 440425.
[2] A. Nawaz, Q. Liu, W. L. Leong, K. E. Fairfull-Smith, P. Sonar, A. Nawaz, Q. Liu, K. E. Fairfull-Smith, P. Sonar, W. L. Leong, *Adv. Mater.* **2021**, *33*, 2101874.
[3] J. Rivnay, S. Inal, A. Salleo, R. M. Owens, M. Berggren, G. G. Malliaras, *Nat. Rev. Mater.* **2018**, *3*, 17086.
[4] A. V. Marquez, N. McEvoy, A. Pakdel, *Molecules* **2020**, *25*, 5288.
[5] A. B. Woeppel, J. Schaefer, H. J. Kim, B. W. Boudouris, S. P. Beaudoin, *ACS Appl. Polym. Mater.* **2022**, *4*, 6667.
[6] A. Koklu, D. Ohayon, S. Wustoni, A. Hama, X. Chen, I. McCulloch, S. Inal, *Sens. Actuators B Chem.* **2021**, *329*, 129251.
[7] A. Koklu, S. Wustoni, K. Guo, R. Silva, L. Salvigni, A. Hama, E. Diaz-Galicia, M. Moser, A. Marks, I. Mcculloch, R. Grünberg, S. T. Arold, S. Inal, A. Koklu, S. Wustoni, K. Guo, R. Silva, L. Salvigni, A. Hama, S. Inal, E. Diaz-Galicia, R. Grünberg, S. T. Arold, M. Moser, A. Marks, I. Mcculloch, *Adv. Mater.* **2022**, *34*, 2202972.
[8] F. Wang, Y. Han, N. Gu, *ACS Sens.* **2021**, *6*, 290.
[9] J. Gao, J. M. Karp, R. Langer, N. Joshi, *Chem. Mater.* **2023**, *35*, 359.
[10] N. Alegret, A. Dominguez-Alfaro, D. Mecerreyes, *Biomacromolecules* **2019**, *20*, 73.
[11] B. Huang, Z. Zhao, Y. Zheng, K. Xu, D. Wang, Q. Yang, T. Yang, X. Yang, H. Chen, *Internat. J. Bioprint. Null* **2024**, *0*, 1725.
[12] K. Betha, C. Imani, J. M. Dodda, J. Yoon, F. G. Torres, G. R. Deen, R. Al-Ansari, K. B. C. Imani, J. Yoon, J. M. Dodda, F. G. Torres, A. B. Imran, G. R. Deen, R. Al-Ansari, *Adv. Sci.* **2024**, 2306784.
[13] M. J. Donahue, A. Sanchez-Sanchez, S. Inal, J. Qu, R. M. Owens, D. Mecerreyes, G. G. Malliaras, D. C. Martin, *Mater. Sci. Engineer.: R: Rep.* **2020**, *140*, 100546.
[14] L. V. Kayser, D. J. Lipomi, *Adv. Mater.* **2019**, *31*, 1806133.
[15] A. Martinelli, A. Nitti, G. Giannotta, R. Po, D. Pasini, *Mater. Today Chem.* **2022**, *26*, 101135.
[16] M. Criado-Gonzalez, A. Dominguez-Alfaro, N. Lopez-Larrea, N. Alegret, D. Mecerreyes, *ACS Appl. Polym. Mater.* **2021**, *3*, 2865.
[17] J. Qu, L. Ouyang, C. C. Kuo, D. C. Martin, *Acta Biomater.* **2016**, *31*, 114.
[18] A. Dominguez-Alfaro, E. Gabirondo, N. Alegret, C. María De León-Almazán, R. Hernandez, A. Vallejo-Illarramendi, M. Prato, D. Mecerreyes, A. Dominguez-Alfaro, E. Gabirondo, N. Alegret, C. M. De León-Almazán, R. Hernandez, D. Mecerreyes, M. Prato, *Macromol. Rapid Commun.* **2021**, *42*, 2100100.
[19] H. Yuk, B. Lu, S. Lin, K. Qu, J. Xu, J. Luo, X. Zhao, *Nat. Commun.* **2020**, *2020*, 1604.
[20] A. Aguzin, A. Dominguez-Alfaro, M. Criado-Gonzalez, S. Velasco-Bosom, M. L. Picchio, N. Casado, E. Mitoudi-Vagourdi, R. J. Minari, G. G. Malliaras, D. Mecerreyes, *Mater. Horiz.* **2023**, *10*, 2516.
[21] B. Lu, H. Yuk, S. Lin, N. Jian, K. Qu, J. Xu, X. Zhao, *Nat. Commun.* **2019**, *10*, 1.
[22] X. Xie, Z. Xu, X. Yu, H. Jiang, H. Li, W. Feng, *Nat. Commun.* **2023**, *14*, 1.
[23] G. Yang, J. Fan, K. Zhang, C. Gu, J. Li, K. Kang, C. Xiang, L. Qian, T. Zhang, G. Yang, J. Fan, K. Zhang, C. Gu, J. Li, K. Kang, C. Xiang, L. Qian, T. Zhang, *Adv. Funct. Mater.* **2023**, 2314983.
[24] O. Dadras-Toussi, M. Khorrami, A. Sam, C. Louis, S. Titus, S. Majd, C. Mohan, M. R. Abidian, O. Dadras-Toussi, M. Khorrami, A. S. C. Louis, S. Majd, C. Mohan, M. R. Abidian, *Adv. Mater.* **2022**, *34*, 2200512.
[25] D. N. Heo, S. J. Lee, R. Timsina, X. Qiu, N. J. Castro, L. G. Zhang, *Mater. Sci. Eng., C* **2019**, *99*, 582.
[26] A. Dominguez-Alfaro, E. Mitoudi-Vagourdi, I. Dimov, M. L. Picchio, N. Lopez-Larrea, J. L. de Lacalle, X. Tao, R. R. M. Serrano, A. Gallastegui, N. Vassardanis, D. Mecerreyes, G. G. Malliaras, *Adv. Sci.* **2024**, 2306424.
[27] J. R. Aggas, S. Abasi, J. F. Phipps, D. A. Podstawczyk, A. Guiseppi-Elie, *Biosens. Bioelectron.* **2020**, *168*, 112568.
[28] X. Ding, R. Jia, Z. Gan, Y. Du, D. Wang, X. Xu, *Mater. Res. Express* **2020**, *7*.
[29] A. Ruggiero, V. Criscuolo, S. Grasselli, U. Bruno, C. Ausilio, C. L. Bovio, O. Bettucci, F. Santoro, *Chem. Commun.* **2022**, *58*, 9790.
[30] V. Bertana, G. Scordo, E. Camilli, L. Ge, P. Zaccagnini, A. Lamberti, S. L. Marasso, L. Scaltrito, *Polymers (Basel)* **2023**, *15*, 2657.
[31] A. Dominguez-Alfaro, M. Criado-Gonzalez, E. Gabirondo, H. Lasa-Fernández, J. L. Olmedo-Martínez, N. Casado, N. Alegret, A. J. Müller, H. Sardon, A. Vallejo-Illarramendi, D. Mecerreyes, *Polym. Chem.* **2021**, *13*, 109.
[32] M. L. Picchio, A. Gallastegui, N. Casado, N. Lopez-Larrea, B. Marchiori, I. del Agua, M. Criado-Gonzalez, D. Mantione, R. J. Minari, D. Mecerreyes, *Adv. Mater. Technol.* **2022**, *7*, 2101680.
[33] S. Ghaderi, H. Hosseini, S. A. Haddadi, M. Kamkar, M. Arjmand, *J. Mater. Chem. A Mater.* **2023**, *11*, 16027.
[34] V. R. Feig, H. Tran, M. Lee, Z. Bao, *Nat. Commun.* **2018**, *9*, 1.

© 2024 The Authors. Advanced Functional Materials published by Wiley-VCH GmbH

16163028, 2024, 40, Downloaded from https://onlinelibrary.wiley.com/doi/10.1002/adfm.202403708 by Universidad Del Pais Vasco, Wiley Online Library on [08/10/2024]. See the Terms and Conditions (https://onlinelibrary.wiley.com/terms-and-conditions) on Wiley Online Library for rules of use; OA articles are governed by the applicable Creative Commons License

[35] Z. Deng, R. Yu, B. Guo, *Mater. Chem. Front.* **2021**, *5*, 2092.
[36] Z. U. Arif, M. Y. Khalid, A. Tariq, M. Hossain, R. Umer, *Giant* **2024**, *17*, 100209.
[37] M. Champeau, D. Alves Heinze, T. Nunes Viana, E. Rodrigues de Souza, A. Cristine Chinellato, S. Titotto, M. Champeau, D. A. Heinze, T. N. Viana, E. R. de Souza, A. C. Chinellato, S. Titotto, *Adv. Funct. Mater.* **2020**, *30*, 1910606.
[38] M. Wei, Y. Gao, X. Li, M. J. Serpe, *Polym. Chem.* **2016**, *8*, 127.
[39] Y. Liu, R. Liu, J. Qiu, S. Wang, *J. Adv. Manuf. Process* **2022**, *4*, e10107.
[40] S. Cao, X. Tong, K. Dai, Q. Xu, *J. Mater. Chem. A Mater.* **2019**, *7*, 8204.
[41] Y. Zhu, S. Liu, X. Shi, D. Han, F. Liang, *Mater. Chem. Front.* **2018**, *2*, 2212.
[42] S. Marina, D. Mantione, K. Manojkumar, V. Kari, J. Gutierrez, A. Tercjak, A. Sanchez-Sanchez, D. Mecerreyes, *Polym. Chem.* **2018**, *9*, 3780.
[43] S. Shang, J. Liu, Y. He, P. Zhu, *Mater. Lett.* **2020**, *272*, 127862.
[44] B. Mutharani, P. Ranganathan, S. M. Chen, *Sens. Actuators B Chem.* **2020**, *304*, 127361.
[45] M. Jia, J. Zhang, *Polymer J.* **2022**, *54*, 793.
[46] J. Mingot, S. Lanzalaco, A. Àgueda, J. Torras, E. Armelin, *Adv. Funct. Mater.* **2023**, 2311523.
[47] P. Xue, C. Valenzuela, S. Ma, X. Zhang, J. Ma, Y. Chen, X. Xu, L. Wang, P. Xue, C. Valenzuela, S. Ma, X. Zhang, J. Ma, Y. Chen, X. Xu, L. Wang, *Adv. Funct. Mater.* **2023**, *33*, 2214867.
[48] M. Garcia-Hernando, J. Saez, A. Savva, L. Basabe-Desmonts, R. M. Owens, F. Benito-Lopez, *Biosens. Bioelectron.* **2021**, *191*, 113405.
[49] J. Liu, J. Liu, F. Ma, J. Liu, *ACS Appl. Polym. Mater.* **2019**, *1*, 152.
[50] A. Matsumoto, H. Kuwata, S. Kimura, H. Matsumoto, K. Ochi, Y. Moro-oka, A. Watanabe, H. Yamada, H. Ishii, T. Miyazawa, S. Chen, T. Baba, H. Yoshida, T. Nakamura, H. Inoue, Y. Ogawa, M. Tanaka, Y. Miyahara, T. Suganami, *Communications Bio.* **2020**, *3*, 1.
[51] S. Chen, H. Matsumoto, Y. Moro-oka, M. Tanaka, Y. Miyahara, T. Suganami, A. Matsumoto, S. Chen, A. Matsumoto, H. Matsumoto, Y. Moro-oka, Y. Miyahara, M. Tanaka, T. Suganami, *Adv. Funct. Mater.* **2019**, *29*, 1807369.
[52] A. Matsumoto, M. Tanaka, H. Matsumoto, K. Ochi, Y. Moro-Oka, H. Kuwata, H. Yamada, I. Shirakawa, T. Miyazawa, H. Ishii, K. Kataoka, Y. Ogawa, Y. Miyahara, T. Suganami, *Sci. Adv.* **2017**, *3*.
[53] J. Y. Li, Y. H. Feng, Y. T. He, L. F. Hu, L. Liang, Z. Q. Zhao, B. Z. Chen, X. D. Guo, *Acta Biomater.* **2022**, *153*, 308.
[54] G. P. Kenny, R. J. Sigal, R. McGinn, *Temperature* **2016**, *3*, 119.
[55] N. Lopez-Larrea, M. Criado-Gonzalez, A. Dominguez-Alfaro, N. Alegret, I. Del Agua, B. Marchiori, D. Mecerreyes, *ACS Appl. Polym. Mater.* **2022**, *4*, 6749.
[56] N. Lopez-Larrea, A. Gallastegui, L. Lezama, M. Criado-Gonzalez, N. Casado, D. Mecerreyes, N. Lopez-Larrea, A. Gallastegui, M. Criado-Gonzalez, N. Casado, D. Mecerreyes, L. Lezama, B. Sarriena, *Macromol. Rapid Commun.* **2024**, *45*, 2300229.
[57] Y. H. Cho, Y. G. Park, S. Kim, J. U. Park, *Adv. Mater.* **2021**, 33.
[58] H. Li, J. Dai, Z. Wang, H. Zheng, W. Li, M. Wang, F. Cheng, *Aggregate* **2023**, *4*.
[59] D. Han, C. Yang, N. X. Fang, H. Lee, *Addit. Manuf.* **2019**, *27*, 606.
[60] D. Mantione, I. del Agua, W. Schaafsma, J. Diez-Garcia, B. Castro, H. Sardon, D. Mecerreyes, *Macromol. Biosci.* **2016**, *16*, 1227.
[61] Z. Chen, J. Li, C. Liu, Y. Liu, J. Zhu, C. Lao, *Ceram. Int.* **2019**, *45*, 11549.
[62] A. Schwab, R. Levato, M. D'Este, S. Piluso, D. Eglin, J. Malda, *Chem. Rev.* **2020**, *120*, 11028.
[63] R. G. Sousa, W. F. Magalhães, R. F. S. Freitas, *Polym. Degrad. Stab.* **1998**, *61*, 275.
[64] Q. T. Pham, Z. H. Yao, Y. T. Chang, F. M. Wang, C. S. Chern, *J. Taiwan Inst. Chem. Eng.* **2018**, *93*, 63.
[65] Q. T. Pham, Z. H. Yao, Y. T. Chang, F. M. Wang, C. S. Chern, *J. Taiwan Inst. Chem. Eng.* **2018**, *93*, 63.
[66] K. H. Son, J. W. Lee, *Materials* **2016**, *9*, 854.
[67] J. H. Park, J. W. Jang, J. H. Sim, I. J. Kim, D. J. Lee, Y. H. Lee, S. H. Park, H. Do Kim, *Int. J. Polym. Sci.* **2019**, *2019*.
[68] J. Šťastná, L. Hanyková, J. Spěváček, *Colloid Polym. Sci.* **2012**, *290*, 1811.
[69] M. B. Browning, S. N. Cereceres, P. T. Luong, E. M. Cosgriff-Hernandez, *J. Biomed. Mater. Res. A* **2014**, *102*, 4244.
[70] W. Li, J. Zhou, Y. Xu, *Biomed. Rep.* **2015**, *3*, 617.
[71] ISO 10993–5:2009 – Biological evaluation of medical devices — Part 5: Tests for in vitro cytotoxicity.
[72] I. M. Basurto, S. A. Muhammad, G. M. Gardner, G. J. Christ, S. R. Caliari, *J. Biomed. Mater. Res. A* **2022**, *110*, 1681.
[73] H. Y. Gong, J. Park, W. Kim, J. Kim, J. Y. Lee, W. G. Koh, *ACS Appl. Mater. Interfaces* **2019**, *11*, 47695.
[74] A. R. Spencer, A. Primbetova, A. N. Koppes, R. A. Koppes, H. Fenniri, N. Annabi, *ACS Biomater. Sci. Eng.* **2018**, *4*, 1558.
[75] B. Yi, Q. Xu, W. Liu, *Bioact. Mater.* **2022**, *15*, 82.
[76] M. Hesam Mahmoudinezhad, A. Karkhaneh, K. Jadidi, *J. Biosci.* **2018**, *43*, 307.
[77] D. N. Heo, S. J. Lee, R. Timsina, X. Qiu, N. J. Castro, L. G. Zhang, *Mater. Sci. Eng., C* **2019**, *99*, 582.
[78] P. Kateb, J. Fan, J. Kim, X. Zhou, G. A. Lodygensky, F. Cicoira, *Flex. Print. Electron.* **2023**, *8*, 045006.
[79] M. Onoda, Y. Abe, K. Tada, *Thin Solid Films* **2010**, *519*, 1230.
[80] P. M. Tsimbouri, L. E. McNamara, E. V. Alakpa, M. J. Dalby, L. A. Turner, *Tissue Engineer.: Second Ed.* **2014**, 217.
[81] Q. Sun, Y. Hou, Z. Chu, Q. Wei, *Bioact. Mater.* **2022**, *10*, 397.
[82] S. R. Huang, K. F. Lin, T. M. Don, C. F. Lee, M. S. Wang, W. Y. Chiu, *J. Polym. Sci. A Polym. Chem.* **2016**, *54*, 1078.
[83] S. Nastyshyn, Y. Stetsyshyn, J. Raczkowska, Y. Nastishin, Y. Melnyk, Y. Panchenko, A. Budkowski, *Polymers* **2022**, *14*, 4245.
[84] Y. Kotsuchibashi, M. Ebara, T. Aoyagi, R. Narain, *Polymers* **2016**, *8*, 380.
[85] T. Q. Nguyen, C. Breitkopf, *J. Electrochem. Soc.* **2018**, *165*, E826.
[86] D. Ohayon, V. Druet, S. Inal, *Royal Soc. Chem.* **2023**, *52*, 1001.
[87] S. L. Bidinger, S. Han, G. G. Malliaras, T. Hasan, *Appl. Phys. Lett.* **2022**, *120*, 73302.
[88] X. Strakosas, M. Bongo, R. M. Owens, *J. Appl. Polym. Sci.* **2015**, *132*, 41735.
[89] F. Benyettou, N. Kaddour, T. Prakasam, G. Das, S. K. Sharma, S. A. Thomas, F. Bekhti-Sari, J. Whelan, M. A. Alkhalifah, M. Khair, H. Traboulsi, R. Pasricha, R. Jagannathan, N. Mokhtari-Soulimane, F. Gándara, A. Trabolsi, *Chem. Sci.* **2021**, *12*, 6037.
[90] D. A. Koutsouras, F. Torricelli, P. Gkoupidenis, P. W. M. Blom, *Adv. Mater. Technol.* **2021**, *6*, 2100732.
[91] N. Fumeaux, C. P. Almeida, S. Demuru, D. Briand, *Sci. Rep.* **2023**, *13*, 11467.
[92] T. Heise, A. Y. Sawyer, T. Hirai, S. Schaible, H. Sy, S. Wickramasekara, *Regul. Toxicol. Pharmacol.* **2022**, *131*, 105164.
[93] D. Ohayon, G. Nikiforidis, A. Savva, A. Giugni, S. Wustoni, T. Palanisamy, X. Chen, I. P. Maria, E. Di Fabrizio, P. M. F. J. Costa, I. McCulloch, S. Inal, *Nat. Mater.* **2019**, *19*, 456.
[94] S. Wustoni, A. Savva, R. Sun, E. Bihar, S. Inal, *Adv. Mater. Interfaces* **2019**, *6*, 1800928.
[95] Y. Zhong, P. D. Nayak, S. Wustoni, J. Surgailis, J. Z. Parrado Agudelo, A. Marks, I. McCulloch, S. Inal, *ACS Appl. Mater. Interfaces* **2023**, *12*, 26.

© 2024 The Authors. Advanced Functional Materials published by Wiley-VCH GmbH

16163028, 2024, 40, Downloaded from https://onlinelibrary.wiley.com/doi/10.1002/adfm.202403708 by Universidad Del Pais Vasco, Wiley Online Library on [08/10/2024]. See the Terms and Conditions (https://onlinelibrary.wiley.com/terms-and-conditions) on Wiley Online Library for rules of use; OA articles are governed by the applicable Creative Commons License